PERFORMANCE IMPROVEMENT OF A PROOF-MASS ACTUATOR USING NONLINEAR CONTROL

by

Gregory Allan Zvonar

Thesis submitted to the Faculty of the

Virginia Polytechnic Institute and State University

in partial fulfillment of the requirements for the degree of

MASTER OF SCIENCE

in

Electrical Engineering

APPROVED:

Douglas K. Lindner, Chairman

Dusan Borojevic

John S. Bay

December, 1991

Blacksburg, Virginia

PERFORMANCE IMPROVEMENT OF A PROOF-MASS ACTUATOR USING NONLINEAR CONTROL

by

Gregory Allan Zvonar

Committee Chairman: Douglas K. Lindner

Electrical Engineering

(ABSTRACT)

In this thesis, the proof-mass actuator is studied for vibration suppression of a flexible structure. While these actuators have a favorable force-to-weight ratio, the finite travel of the proof-mass, called the stroke length, imposes restrictions on the use of the actuator. This restriction implies that the actuator has a finite operating region in terms of initial conditions on the state. This operating region, along with the amount of vibration suppression potential, defines the performance of the actuator.

To increase the performance, nonlinear control is proposed. These control laws monitor the position and velocity of the proof-mass and apply a large restoring force whenever the proof-mass is in danger of breaking its stroke limit. A harmonic balance analysis concludes that these nonlinear control laws do not induce limit cycles. The performance of actuators with different parameters is also compared. A relation is presented that associates the modal frequency of the structure to these parameters. It is also found that large stroke with small mass offers the best performance with the nonlinear control in place.

ACKNOWLEDGEMENTS

I would like to thank all of my friends and family for their encouragement throughout my graduate career. I want to especially thank Tonya. She was always behind me and gave me perseverance to complete this thesis. My parents were also a great source of strength. I will always be indebted to them for their constant support.

I would also like to thank everyone on my committee. Dr. Lindner was an excellent advisor - always nudging me back on track and showing the way whenever I got caught up in troublesome details. Dr. Borojevic was always full of creative and insightful suggestions. I would like to thank Dr. Bay for being a friend and as well as a great technical advisor both in my research and in writing this thesis.

Finally, this work would not have been possible if not for the generous financial support of Mrs. Via. I would like to extend my most sincere appreciation to her as well as all those who were involved in my selection for the Bradley Fellowship.

TABLE OF CONTENTS

LIST OF ILLUSTRATIONS

LIST OF TABLES

CHAPTER 1

INTRODUCTION

The development of large space structures has received a lot of attention lately. These structures present unique challenges for all disciplines in engineering. Not only must these structures be made of strong materials, but since they must be launched into space, the material must be lightweight also. New composite materials can meet these requirements. Due to disturbances such as gravitational forces, docking space shuttles and temperature gradients, these flexible structures will tend to oscillate at large amplitudes. This vibration is undesirable for many reasons such as antennae tracking requirements, structural stress, and human discomfort.

It has been found that active control offers at least a partial solution (Nurre, et. al.). Active vibration suppression would apply forces into the structure to reduce or stop the vibrations. Active control of these vibrations offers an advantage over passive means due to their light weight. The forces are applied by the control system into the structure through a device called an actuator. Examples of actuators considered for vibration suppression of large space structures include gyrodampers, piezoelectrics and reaction jets (Ide, 1988). The most popular is the inertia-type actuators. This type of actuator uses the inertia of a mass to impart forces or torques into the structure. Once such actuator is the reaction wheel actuator

(Anderson and Groom, 1975). The reaction wheel actuator accelerates or decelerates a spinning mass in order to input torques into the structure.

This text deals with a translational version of the reaction wheel actuator called the proof-mass actuator (özgüner, et. al., 1987, Sulla, et. al., 1990, Lindner, 1991). By electromagnetically accelerating a proof-mass on a track, a reaction force is transmitted through the actuator and into the structure. Research performed at Virginia Polytechnic Institute and State University (Clark and Robertshaw, 1989) suggested that proof-mass actuators provide the same amount of vibration suppression as reaction wheel actuators, but with less weight. Unfortunately, proof-mass actuators have a limitation not encountered in the reaction wheel actuator. Since the actuator utilizes a translating mass, its motion is confined to a finite length, called the stroke. One way to circumvent this problem is to construct the stroke to be very large.

An alternative approach to the limited stroke problem is to integrate the size of the stroke into the design. Politansky and Pilkey (Politansky and Pilkey, 1989, Haviland et al, 1990) approached this problem through optimal control arguments. This text presents an alternative method. By finding the conditions under which the actuator does not reach the end of it stroke, an operating region is realized. The size of the stroke is integrated into the design by relating this operating region to the control of the actuator.

The objective of this research is to find a control for the actuator that expands the operating region without increasing the actuator's size. This problem is solved in a two part fashion. First, a linear control system is designed that takes into account the length of the stroke. A majority of the design for the linear control comes directly from (Celano, 1989). There the linear control system of the actuator

is designed so that the actuator produces the largest possible force given the actuator's physical limitations.

In the next step, the operating region is further expanded by augmenting the linear design with nonlinear control. Finding a control that significantly expands the operating region, even when starting from physical considerations, is more or less a trial and error process. Of the numerous forms attempted, only a few expand the operating region satisfactorily. In order to evaluate the designs, a measure of the performance is required. The performance of the control system is not only related to the size of the operating region, but also to the vibration suppression capabilities. That is, the new control system must not only expand the operating region but also it must not sacrifice how well the structure is controlled. In this thesis, a performance function is defined. A plot of this function is used to compare systems containing different actuators and control laws.

Since the actuator and its control are nonlinear, an analysis is included to predict the possibility of limit cycles. The results from this analysis indicate which control systems can be used to avoid limit cycles.

It should be noted that the discussions in this paper are system level oriented and do not address implementation issues. The issues engaged in this paper are present in any proof-mass realizations. In addition, since the performance of an actuator depends on its placement on the structure, this problem will be avoided by studying various actuator on the same structure model and located at an unchanging location.

In summary, this text demonstrates a method to evaluate a proof-mass actuator control systems for vibration suppression, provides nonlinear control laws that expand the operating region, offers guidelines for the design of basic actuator

attributes, such as stroke length, and details the design of the overall control system.

In Chapter 2, the models of the actuator and structure are developed as well as the design of the linear control systems. A performance measure is devised in Chapter 3. The nonlinear control laws to expand the operating region are presented in Chapter 4. In Chapter 5, the actuator parameters are varied and performance is evaluated with the aid of the damping plot. In Chapter 6, a limit cycle analysis is performed on the system. Finally, conclusions and suggestions for future work are offered in Chapter 7.

CHAPTER 2

MODEL DEVELOPMENT AND LINEAR DESIGN

1. Actuator Model

Consider a linear DC motor (Ham et. al., 1989) in Figure 1, as a proof-mass actuator.

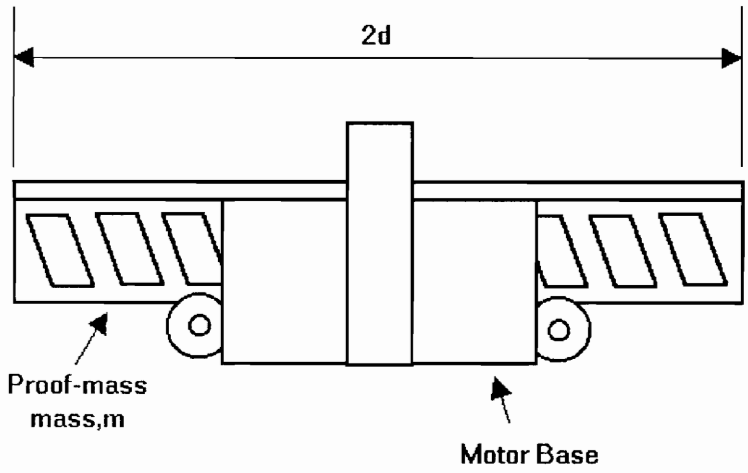

Figure 1. The Linear D.C. Motor

This actuator consists of motor base and a proof-mass of mass m and length 2d. Thus the actuator has a stroke of d. The position of the center of the proof-mass with respect to an inertial reference frame is denoted y(t) as shown in Figure 5. The motor base contains the motor coils and the power electronics. Assume that the actuator contains internal current compensation loops so that the electromagnetic force on the proof-mass, f_{pm}, is proportional to the input control signal, v(t). i.e:

$$f_{pm}(t) = K_F \cdot v(t) \tag{2.1.1}$$

Neglecting friction between the motor base and the proof-mass, the model of the proof-mass motion is:

$$m \cdot \ddot{y}(t) = f_{pm}(t) = K_F \cdot v(t) \tag{2.1.2}$$

Due to the limitations of the electrical system, the actuator will only be able to produce a maximum force, F_{Max}. This limitation in the actuator can be modeled by a saturation function. The saturation function, $S_T(\sigma)$, is defined as:

$$S_T(\sigma) = \begin{cases} T, & \sigma > T \\ \sigma, & -T \le \sigma \le T \\ -T, & \sigma < -T \end{cases} \tag{2.1.3}$$

The force limit has $T = F_{Max}$ and $\sigma = K_F\, v(t)$. The block diagram of this open loop actuator model is identified as the "linear motor" in Figure 2.

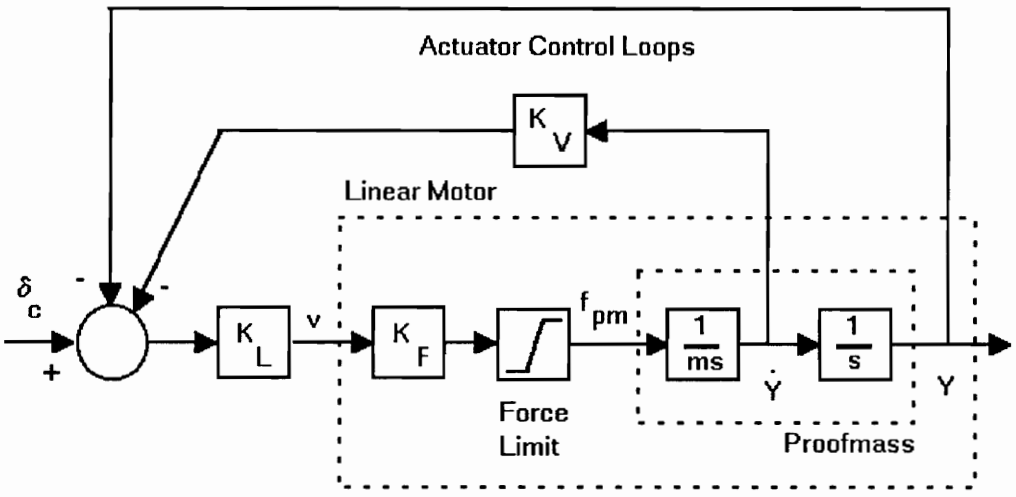

Figure 2. Proof-Mass Actuator

Assume that the actuator is instrumented with a position sensor in the motor base and an inertial velocity sensor on the proof-mass. An inertial velocity measurement can be obtained by integrating the output of an accelerometer mounted on the proof-mass. Herein, it will be assumed that the transfer function of

this sensor is frequency independent. For an analysis of this system accounting for the dynamics of an accelerometer and integrator see (Celano, 1989). This paper will present numerical simulations of this actuator. Unless otherwise noted, the basic actuator parameters used for these simulations are shown in Table 1.

Table 1. Actuator Parameters

Proof-mass Mass, m	3 kg
Force Limit, F_{MAX}	30 N
Stroke Limit, d	.15 m
Force Conversion Constant, K_F	1 N/V

2. Design of the Actuator Control Loops

Note that proof-mass actuator is not open loop BIBO stable. The actuator can be stabilized by feeding back the signals from the actuator sensors with a velocity feedback gain of K_V and a forward gain of K_L. These two feedback loops are called here the actuator control loops and are identified in Figure 2.

The actuator control loops will be designed to allow the actuator to perform to its maximum potential. The largest force that a proof-mass actuator can exert is bound by its physical parameters. These limitations stem from two physical parameters: the maximum displacement of the proof-mass (the stroke limit d) and the maximum capability of the power electronics (the force limit, F_{Max}). These force constraints can be described in terms of the sinusoidal steady state operation (Lindner, et al., 1991) and are modelled by a frequency depended function.

The first limitation of the force is due to the limited length of the stroke. If the proof-mass is moving in a sinusoidal manner at constant frequency, then

certainly the larger the amplitude of this motion, the larger the force exerted on the structure. Thus, the extreme case of the proof-mass moving at its stroke limit produces a maximum force. That is, if the motion of the proof-mass is:

$$y(t) = d \cdot \sin(\omega \cdot t) \tag{2.2.1}$$

then the maximum instantaneous force is:

$$F_{\text{Max Stroke}} = md\omega^2 \tag{2.2.2}$$

If the actuator is attached to a structure, (2.2.2) is approximately true assuming the effective mass of the structure is much greater than the mass of the proof-mass (Lindner, et al., 1991). This limitation versus frequency is plotted on a log-log plot in Figure 3 as "Stroke Saturation."

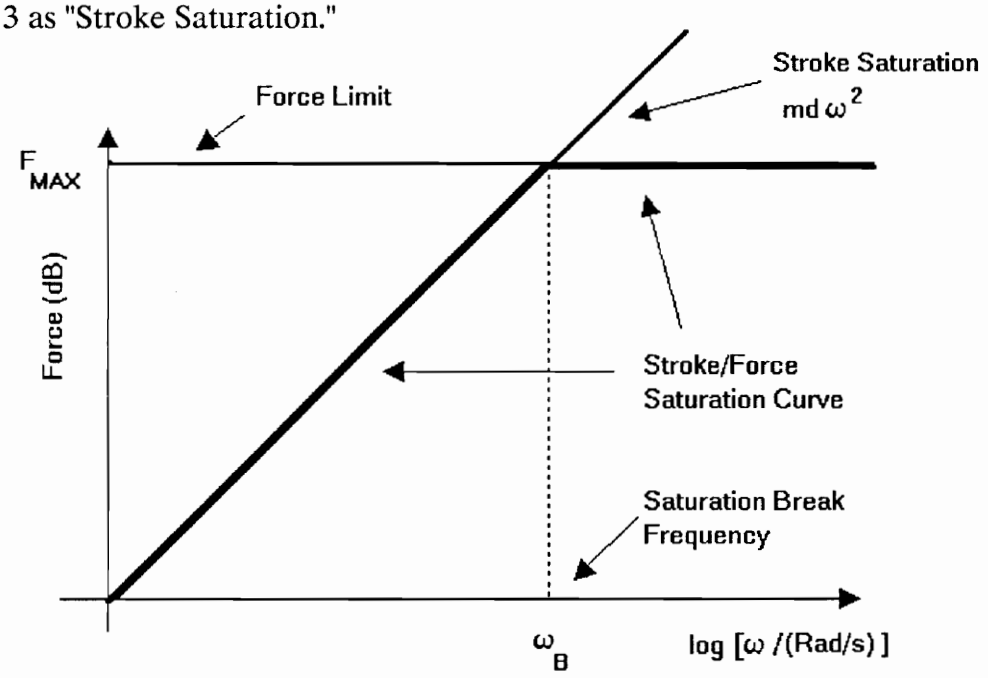

Figure 3. Frequency Dependent Saturation Curves

The other limitation on the force is due to the power electronics in the actuator. From (2.1.3) the maximum force applied to the proof-mass is denoted

F_{Max}. This limitation is constant with respect to the frequency and is noted in Figure 3 as "Force Limit". The force limit and stroke saturation curves represent the maximum linear capability of the actuator.

At any particular frequency, the maximum force output is the minimum value of these two lines. The frequency at which these lines cross is called the saturation break frequency, ω_B, and is defined as:

$$\omega_B = \sqrt{\frac{F_{Max}}{md}} \tag{2.2.3}$$

At frequencies below the saturation break frequency, ω_B, this maximum force output is determined by stroke length, d, and the mass, m, of the proof-mass, as shown in (2.2.2). Above the saturation break frequency the maximum force output is determined by the maximum available force from the electrical subsystem, F_{Max}. These two force constraints can be combined together to form the stroke/force saturation curve, $C_{s/f}(\omega)$, defined as:

$$C_{s/f}(\omega) = \begin{cases} md\omega^2, & \omega \le \omega_B \\ F_{Max}, & \omega \ge \omega_B \end{cases} \tag{2.2.4}$$

The stroke/force saturation curve and the saturation break frequency are shown in Figure 3. To ensure that the actuator uses all of its force in sinusoidal steady state as determined by (2.2.4), the magnitude of the frequency response of the command-to-force transfer function, from Figure 2,

$$\frac{f_{pm(s)}}{\delta_c(s)} = \frac{K_L K_F\, ms^2}{ms^2 + K_V K_L K_F\, s + K_L K_F} \tag{2.2.5}$$

is matched to the stroke/force saturation curve (Lindner, et al., 1991). This is necessary since if the frequency response curves of (2.2.5) fall below the stroke/force saturation curve, then the actuator is not being commanded to operate at full capacity. On the other hand, if the bandwidth of the actuator is significantly

beyond the stroke/force saturation curve, the actuator will not be able to operate in sinusoidal motion due to the force limit.

To match the magnitude of (2.2.5) to (2.2.4) the gains K_L and K_F are set to:

$$K_L K_F = m\,\omega_B^2$$

$$K_V = \frac{1.4}{\omega_B} \qquad (2.2.6)$$

for a damping of $\zeta = 0.7$. Once this is done the poles of (2.2.5), also called the "poles of the actuator", will have the same frequency as the saturation break frequency, ω_B. It will be assumed from here on that the gains in the actuator control loops are chosen in this manner. The saturation break frequency and the corresponding control gains from the parameters in Table 1 are listed in Table 2. Figure 4 shows the frequency response of the command-to-force transfer function from (2.2.5) for these values. Note that the magnitude closely represents the stroke/force saturation curve.

Table 2. Saturation Break Frequency and Actuator Control Gains

Saturation break Frequency, ω_B	8.165 Rad/s
Loop Gain, K_L	200
Actuator Velocity Gain, K_V	.17146

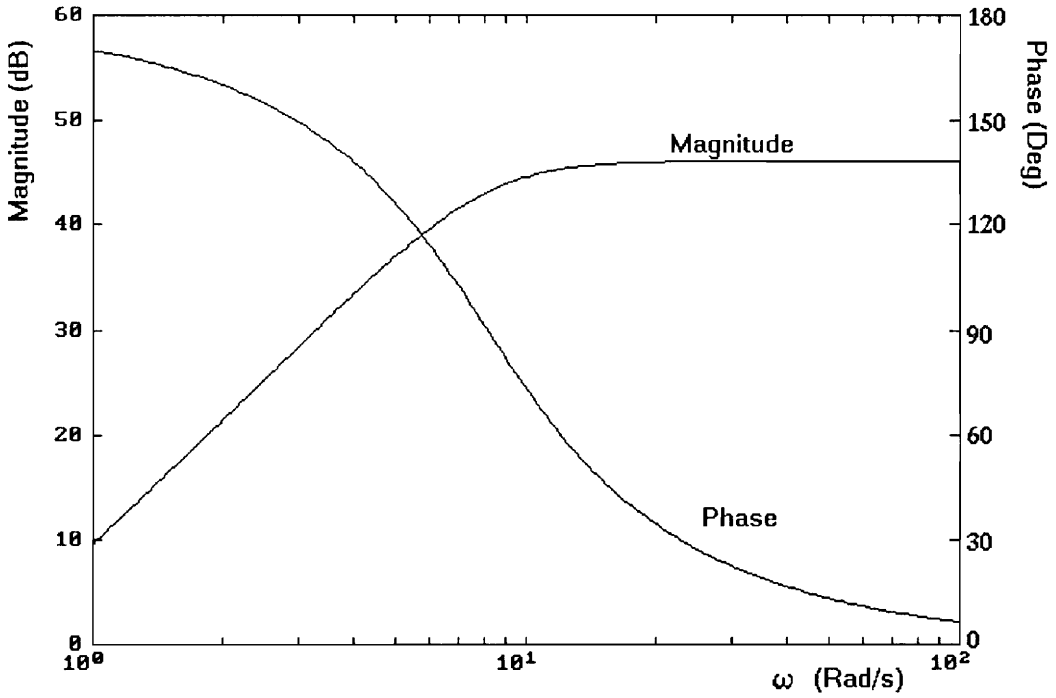

Figure 4. Frequency Response of the Command-to-Force Transfer Function

3. Structure Model

Consider the proof-mass actuator discussed in the last section attached to a simple cantilevered beam as shown in Figure 5. Let p(t) be the displacement of the structure at the point of attachment to the actuator. Here it is assumed that the displacement of the beam is small compared to its length. Thus only a one dimensional displacement is included in model of the beam. For larger displacements, other dynamics such as rotation of the tip would have to be modelled as well.

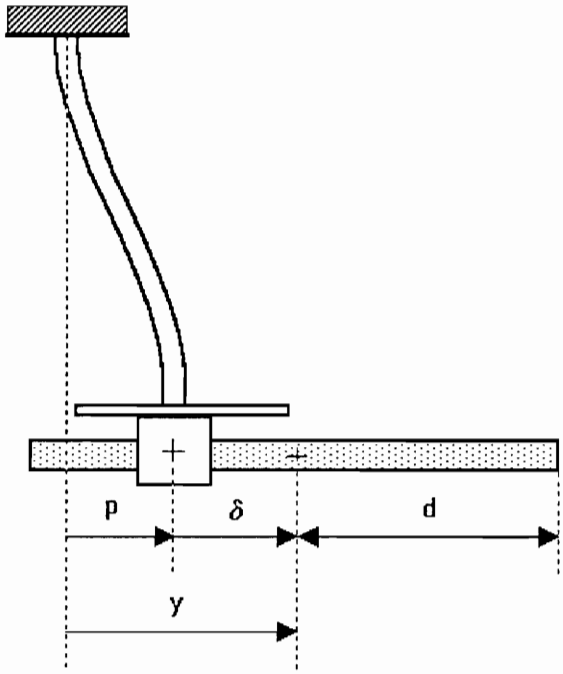

Figure 5. Proof-Mass Actuator Attached to a Flexible Structure

If the structure is modelled by a single vibrational mode, we have,

$$\ddot{\eta}(t) + 2\zeta\omega_s\dot{\eta}(t) + \omega_s{}^2\eta(t) = b\, f_{st}$$
$$\dot{p}(t) = c\, \dot{\eta}(t) \qquad (2.3.1)$$

where $f_{st}(t)$ is the force applied to the structure, $\eta(t)$, is the modal amplitude, ζ is the damping constant, ω_s is the modal frequency, and b and c are the modal influence coefficients. If the structure is modelled with multiple modes, the equation becomes,

$$\ddot{\boldsymbol{\eta}}(t) + 2\begin{bmatrix} \zeta_1\omega_1 & 0 & \dots & 0 \\ 0 & \zeta_2\omega_2 & 0 & \\ \vdots & 0 & \ddots & 0 \\ 0 & \dots & 0 & \zeta_i\omega_i \end{bmatrix}\dot{\boldsymbol{\eta}}(t) + \begin{bmatrix} \omega_1{}^2 & 0 & \dots & 0 \\ 0 & \omega_2{}^2 & 0 & \\ \vdots & 0 & \ddots & 0 \\ 0 & \dots & 0 & \omega_i{}^2 \end{bmatrix}\boldsymbol{\eta}(t) = \mathbf{b}\, f_{st}$$

$$\dot{p}(t) = \mathbf{c}\, \dot{\boldsymbol{\eta}}(t) \qquad (2.2.1)$$

Where i is the number of modes and **b** is a (i x 1) vector constant, **c** is a (1 x i) vector

constant and $\eta(t)$ is a (i x 1) vector function.

Unless otherwise noted, the structure will be assumed to be a single mode structure with parameters listed in Table 3. These values were extracted from a finite element model of the COFS-I Mast (Ham, et al., 1989).

Table 3. Structure Parameters

Natural Frequency, ω_s	8.168 rad/s
Damping, ζ	0.3 %
Actuator/Sensor Coefficients, b,c	0.0240

The structure is instrumented with an inertial velocity sensor and a position sensor colocated at the point of attachment of the actuator. The inertial velocity measurement of the structure could be obtained with an accelerometer and integrator pair as is done in the actuator.

When the model of the structure is combined with the model of the actuator the block diagram in Figure 6 is obtained, where:

$$\frac{\dot{p}(s)}{f_{st}(s)} = H(s) \qquad (2.3.3)$$

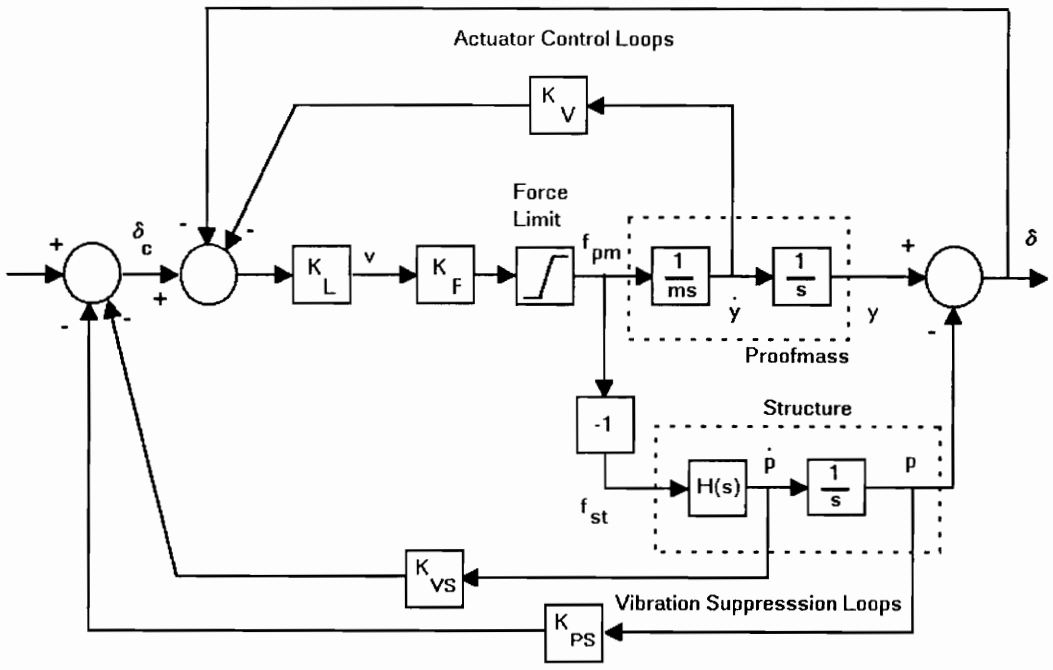

Figure 6. Block Diagram of the Actuator and Structure

The force applied to the proof-mass exerts an equal and opposite force on to the structure. This property is modelled as a negative unity gain block in the block diagram in Figure 6. Note that the position sensor in the actuator measures the displacement of the proof mass from the base, called the relative position. This signal $\delta(t)$ in Figure 6 is defined as:

$$\delta(t) = y(t) - p(t) \tag{2.3.4}$$

This displacement is illustrated in Figure 5. Note from Figure 5 that the relative position has a maximum absolute value of the stroke limit, d. Like the relative position, the relative velocity, $\nu(t)$, between the proof-mass and the structure can be defined as:

$$\nu(t) = \dot{y}(t) - \dot{p}(t) \tag{2.3.5}$$

4. Design of the Vibration Suppression Loops

In order to suppress vibrations in the structure described in the last section, the position and velocity of the structure are fed back to the input of the proof-mass actuator. These loops are identified in Figure 6 as the "vibration suppression loops". In this section, a procedure called "phase compensation" (Lindner, 1991) will be applied to the design of the vibration suppression gains.

The goal in phase compensation is to design a compensator in the feedback loop such that by increasing the gain of the compensator from zero, the damping in the structure poles increases. The vibration suppression loops in Figure 6 can be replaced by an equivalent single loop with compensator. To this end, through block diagram manipulation, the K_{vs} loop is eliminated and the gain in the K_{ps} loop is replaced with the following compensator:

$$C(s) = K_{vs}\, s + K_{ps} \tag{2.4.1}$$

Consider a root locus of the system with C(s) constant, that is zero phase. As this constant is increased from zero, the poles will move through their root loci. Let ϕ_i equal the angle of departure from the poles of the open loop system, p_i, where i = 1 to 4. For low values of C, the best damping enhancement occurs when ϕ is close to 180 degrees for the poles that correspond to the structure dynamics.

If C(s) is dynamic as in (2.4.1), then, from standard classical control theory, the departure angle for pole p_i is:

$$\phi_{di} = \phi_i + \arg(C(p_i)) \tag{2.4.2}$$

If the structure's poles are close to the $j\omega$ axis, that is low damping, then:

$$\arg(C(p_k)) \approx \arg(C(j\omega_s)) \tag{2.4.3}$$

where k = 1,2. The poles p_k correspond to the structure's poles, and ω_s is the structure's modal frequency. By using (2.4.2) and (2.4.3), the phase of (2.4.1) is

easily determined since ϕ_{di} should be around 180 degrees. The magnitude of (2.4.1) is then adjusted through the use of the root locus to acquire the desired damping. By knowing the magnitude and phase of (2.4.1) the values for K_{ps} and K_{vs} can be easily calculated.

Through the use of this phase compensation, the following guidelines for the vibration suppression gains are found. There exists three different relationships between the poles of the structure and the poles of the actuator.

Type 1. Assume that the frequency of the structure's poles is significantly less than the frequency of the actuator. As demonstrated in Figure 7, this results in an angle of departure, ϕ, around 90 degrees. To shift this angle of departure to 180 degrees, the phase of (2.4.1) needs to be around 90 degrees. This is achieved with K_{ps} set to zero and positive values of K_{vs}. Which is equivalent to negative velocity feedback.

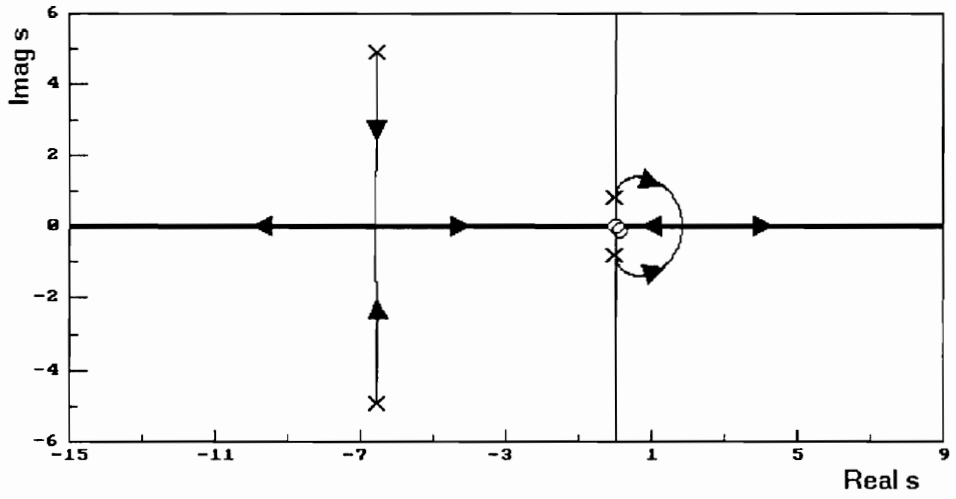

Figure 7. Type 1: Structure Poles Less than Actuator Poles

Type 2. In this case the frequency of the structure's poles and the frequency of the actuator poles are approximately equal. As shown Figure 8, ϕ is approximately

equal to 0 degrees. Thus, phase compensation calls for K_{vs} to be set to zero and to use negative values of K_{ps}, that is positive position feedback.

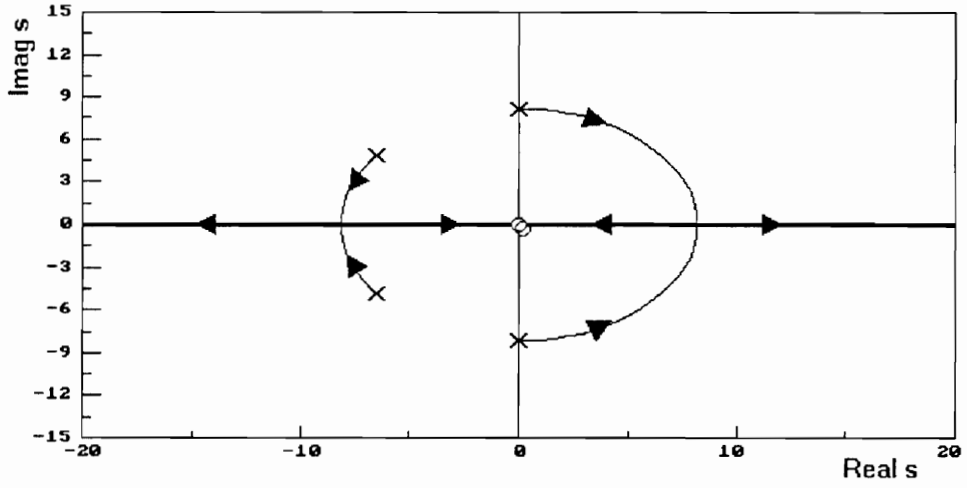

Figure 8. Type 2: Structure Poles Equal to Actuator Poles

Type 3. Finally, if the frequency of the structure's poles is larger than the frequency of the actuator poles, as demonstrated in Figure 9, the angle of departure of the structure's poles is around 270 degrees. This departure angle can be compensated to 180 degrees by using negative values for the K_{vs} gain and setting K_{ps} to zero. Otherwise known as positive velocity feedback.

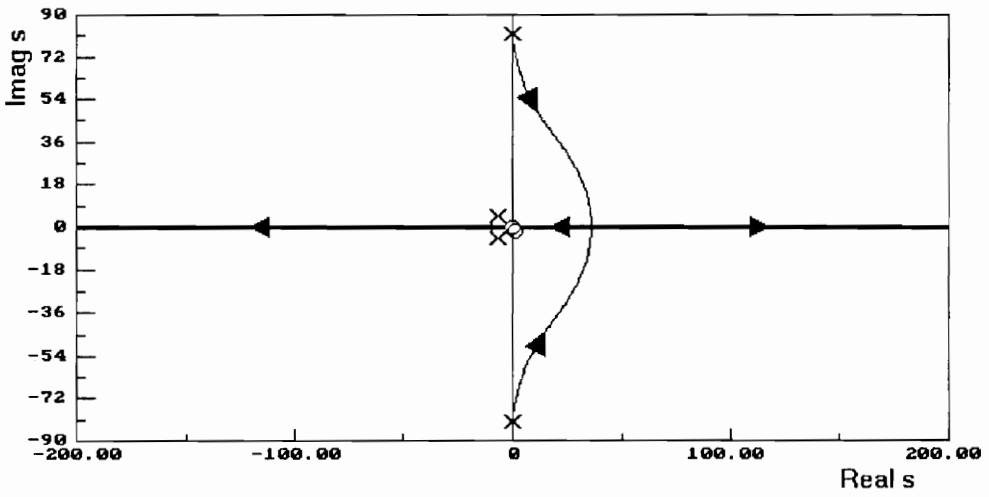

Figure 9. Type 3: Structure Poles Greater than Actuator Poles

Although this development is carried out on a single mode structure, it can also be expanded to multi-modal structures. It this case, the gains in the vibration suppression loops in Figure 6 might have to be replaced with dynamic compensators in order for all the departure angles of the modes to be around 180 degrees. If the system is restricted to the structure of Figure 6, then only the modes greater than or equal to the actuator poles can have their damping increased. This can be seen by combining Type 2 and Type 3 and using an set of negative values for K_{vs} and K_{ps} where the magnitude to K_{ps} is about twice the magnitude of $K_{vs}\omega_B$. Once these gains are properly chosen, the departure angles for the modes greater than or equal to the actuator poles will be close to 180 degrees. The modes less than the actuator poles will move parallel to the $j\omega$ axis at a departure angle of -90 degrees. Thus for small gains, the entire structure will remain stable. Any other combination of the above types will cause some mode to depart into the right half plane.

For a numerical illustration, the design techniques developed in this chapter will now be applied to an actuator/structure system. Consider an actuator with parameters shown in Table 1 and actuator control gains listed in Table 2.

An arbitrary design goal is set to 5% damping in the structure. The vibration suppression loop gains can be calculated using phase compensation techniques. Since the structure's natural frequency, ω_s, is close to the actuator's break frequency, ω_B, this example corresponds to Type 2 above. By following this procedure, the gain K_{vs} is set to zero. The K_{ps} gain for 5% damping in the structure is calculated using root locus techniques, as shown in Figure 10. The values for the vibration suppression gains are shown in Table 4. An open and closed loop initial condition simulation is shown Figure 11 and 12 to demonstrate the damping enhancement.

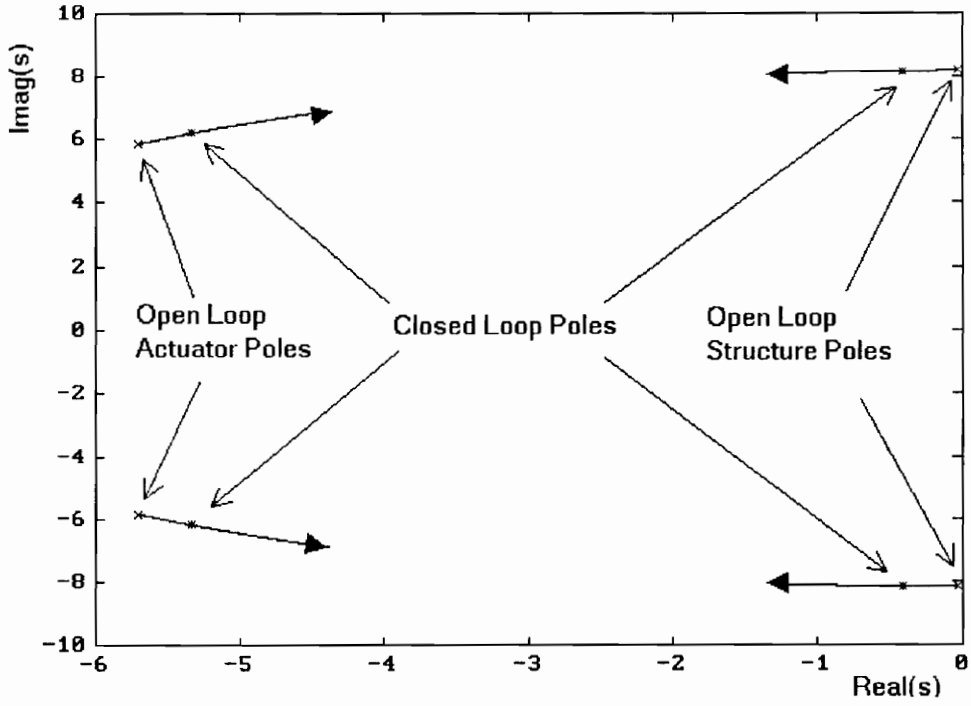

Figure 10. Root Locus of $-K_{ps}$ with K_{vs} Set to Zero

Table 4. Vibration Suppression Gains	
Structure Velocity Gain, K_{vs}	0
Structure Position Gain, K_{ps}	-69.8

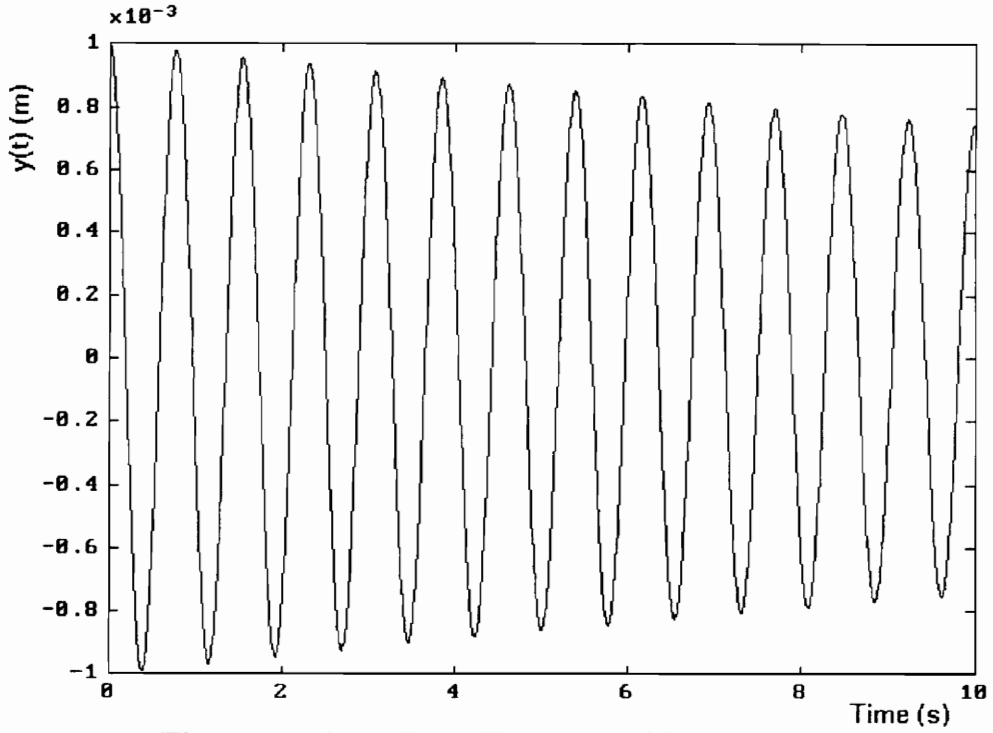

Figure 11. Open Loop Response of Structure Position

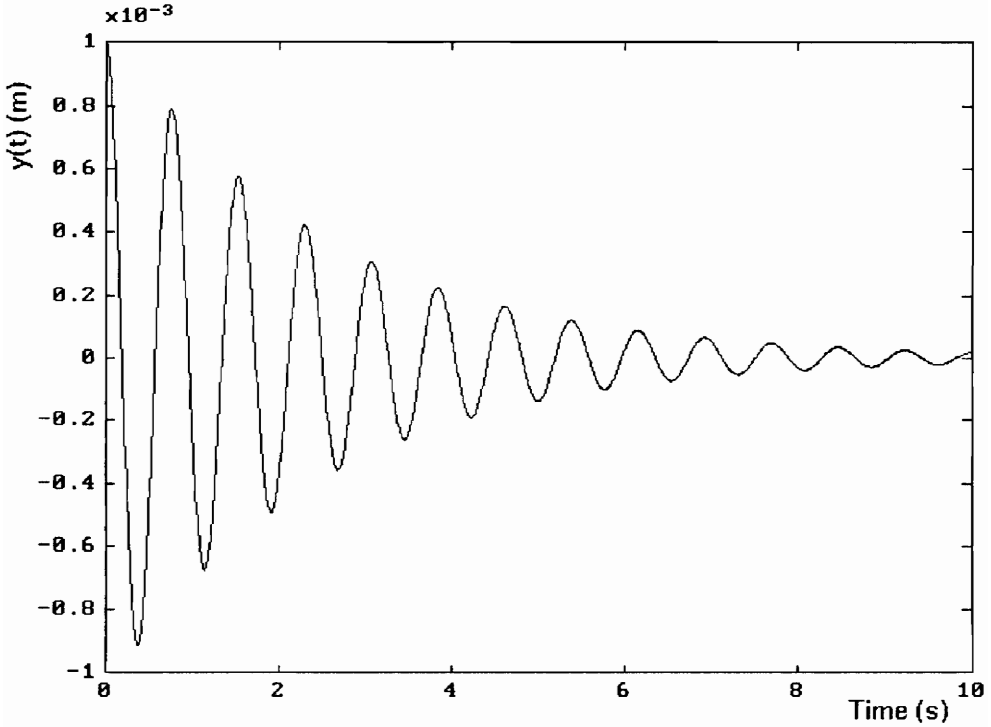

Figure 12. Closed Loop Response of Structure Position

CHAPTER 3

PERFORMANCE CRITERIA

When a proof-mass actuator is attached to a flexible structure, a force applied to the proof-mass will be applied equally and in an opposite direction to the flexible structure. The actuator can operate in this capacity, however, only if the proof-mass does not encounter its stops; that is, the relative displacement of the proof-mass is less than d. If the proof-mass relative displacement is greater than d, it is said that the actuator has saturated in stroke. It is assumed that the actuator is not allowed to saturate in stroke because of possible damage to the device and because high frequency disturbances imparted to the structure. In this chapter, the performance function will be developed which will incorporate the no stroke saturation requirement along with the objective of damping enhancement in the structure. This performance function will be used to study the operating region of the actuator subject to nonlinear constraints.

1. The Performance Function

The restriction that the proof-mass may not saturate in stroke implies that the states of the system must be confined to a subset of the state space. In other words, the actuator has an operating region in the state space of the system. Here this operating region is defined as follows. If the state variables of the model are:

$$x = \begin{bmatrix} y \\ \dot{y} \\ p \\ \dot{p} \end{bmatrix} \tag{3.1.1}$$

The the operating region, $\mathcal{OR}$, is the set of initial conditions, x_0, such that:

$$\mathcal{OR} = \left\{ x_0 = x(0) \;\middle|\; \max_{t \geq 0} |\delta(t)| \leq d \right\} \tag{3.1.2}$$

That is, given an initial condition on the system, if the actuator does not saturate in stroke throughout the response, the initial condition is in the operating region. The operating region reflects the capacity of the actuator to control transient disturbances. Clearly, the larger the operating region, the better the performance of the actuator.

The performance also depends also on how well the actuator suppresses vibrations in the structure. However the "damping" for a nonlinear system does not have a standard definition. Furthermore, its value will vary from initial condition to initial condition. The notion of damping is extended to nonlinear systems for each initial condition x_0 by defining a value similar to the log decrement of the structure's position. Let $t_s(x_0)$ be the 1% settling time of the structure's position trajectory corresponding to the initial condition x_0. Define the equivalent damping, $\zeta(x_0)$, as:

$$\zeta(x_0) = \frac{-\ln 0.01}{\omega_s t_s(x_0)} \tag{3.1.3}$$

For a linear system this definition of damping will coincide with the usual definition of damping for all initial conditions. Note that the settling time is calculated from a simulation of p(t) similar to that of Figure 12.

The performance of this system is summarized by the performance function, ζ_{PM}, as:

$$\zeta_{PM} : \mathbb{R}^4 \rightarrow \mathbb{R}; \quad \zeta_{PM}(x_0) = \begin{cases} \zeta(x_0), & x_0 \in \mathcal{OR} \\ 0, & x_0 \notin \mathcal{OR} \end{cases} \tag{3.1.4}$$

Since the structure has some open loop damping, the equivalent damping will never be zero in the operating region, assuming that no limit cycles are generated. Thus, a plot of this function will identify the operating region of the actuator and the performance of the vibration suppression through equivalent damping in the operating region.

Note that the performance function is defined on a 4-dimensional domain. In order to view this function, it is plotted on the subspace of initial conditions where:

$$y(0) = p(0) \quad \text{and} \quad \dot{y}(0) = \dot{p}(0) \tag{3.1.5}$$

On this subspace the initial relative position and the relative velocity are zero. This subspace is chosen since the initial value of the relative position never violates the stroke limit. This subspace serves as a basis of comparison for different actuators with widely varying parameters. Figure 13 shows a graph of the performance function, called the damping plot. Note that each point of the function represents a separate simulation of the system. A flowchart of the algorithm to compute this function is contained in Appendix.

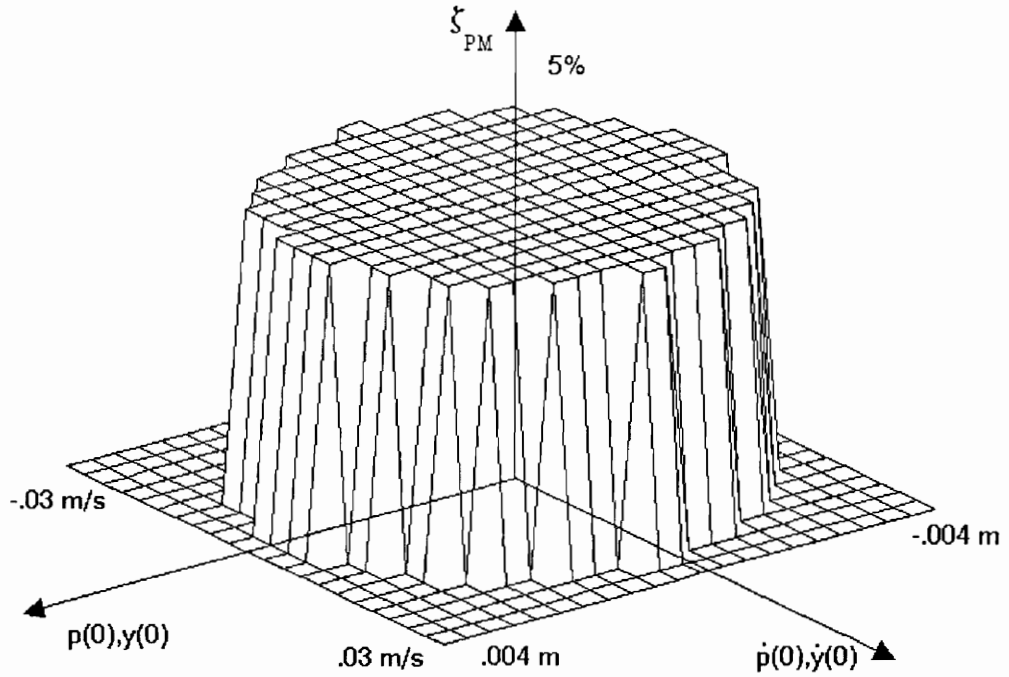

Figure 13. Performance Function

The performance function in Figure 13 will be the baseline comparison for all other damping plots in this text. This plot was created from the system shown in Figure 6 whose values are shown in Tables 1 through 4. This system will be referred to as the "linear design". The next chapter will demonstrate various nonlinear control laws that improve the performance of the system compared with this damping plot.

CHAPTER 4

PERFORMANCE IMPROVEMENT WITH NONLINEAR CONTROL

The operating region of the proof-mass actuator system could be easily expanded by extending the stroke or increasing its mass. But from (2.2.2), this would mean the actuator is now capable of delivering more force. Therefore, the actuator is oversized and not being used to its full capability.

This chapter explores another option. The operating region is expanded, increasing performance, by using nonlinear control. The performance of the nonlinear systems will be evaluated with respect to the linear design with the aid of the damping plot.

1. Command Limiter

Note that if the system in Figure 2 has a high loop gain, the system is considered a "relative position commanded system" due to the unity feedback from the relative position. That is, if the input frequencies are low, the output amplitude will be approximately equal to the input amplitude. Thus, the input of the system, δ_c, represents the desired, or commanded, output. Because the actuator is a relative position commanded system, we have the following property:

$$\delta_c = A \sin \omega t \quad \Rightarrow \quad \sup |\delta| \approx A , \quad \text{if} \quad \omega < \omega_B \tag{4.1.1}$$

For frequencies larger than ω_B the amplitude of δ would be less than A. It is clear then in order to prevent large values of A from causing stroke saturation, a command limiter, $S_{\delta_{cmax}}(\sigma)$, (see (2.1.3)) should be inserted before δ_c as shown in Figure 14.

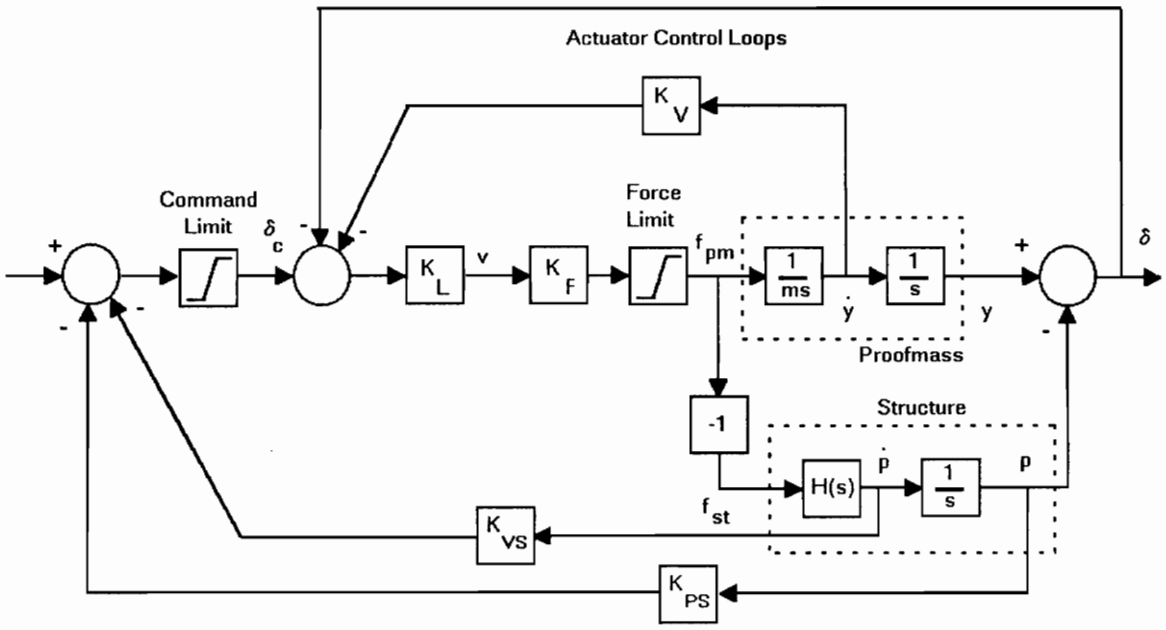

Figure 14. Command Limiter

The value of δ_{cmax} could be thought of as a control design variable, in which the size of the operating region could be traded off against the equivalent damping. An obvious upper bound for δ_{cmax} is d, the stroke limit. This would prevent the vibration suppression loops from commanding the proof mass beyond its stroke limit.

Consider this control applied to the linear design. The performance function of this system with the command limiter added with δ_{cmax} = 0.15 m is shown in Figure 15. Compared with Figure 13, which is the performance function of the

linear design, the size of the operating region is increased with only a slight loss in the equivalent damping at the edges of the operating region.

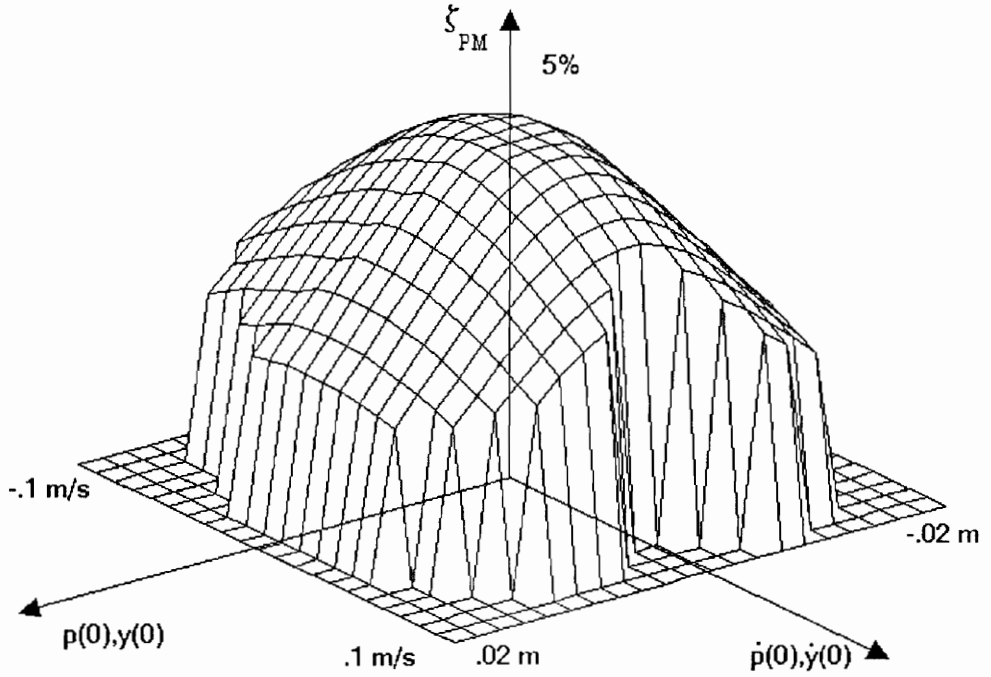

Figure 15. Performance Function Using a Command Limiter

Note that the maximum value of the performance function is 5%. This is the damping enhancement provided by the linear vibration suppression loops. The nonlinear control laws presented in this chapter function only to increase the operating region, not to provide additional equivalent damping.

Through the use of the command limiter, the operating region has indeed been increased. To further increase the operating region, the actuator's input must be altered whenever the proof mass is in danger of stroke saturation. Nonlinear feedback can be employed for this purpose. These loops will be added to the present system shown in Figure 14.

2. Stiff Spring Control

The proof-mass actuator with its actuator control loops in place acts similar to mass/spring/damper system. The amplitude of this type of system can be limited through the use of a stiff spring. A stiff spring will apply a larger restoring force as the proof-mass approaches the end of its stroke. From this physical considerations, one candidate for nonlinear control is to supplement the position feedback loop with nonlinear feedback simulating a stiff spring. Consider the function:

$$f_1(\delta) = \frac{K_1\,\delta}{(d - |\delta|)^2}, \quad K_1 = 2 \times 10^{-4} \tag{4.2.1}$$

This function is close to zero except near the stroke limits where it grows unbounded. These singularities are not a problem since the proof-mass is never allowed to break its stroke limit. When this function is added to the linear position feedback loop, the proof-mass acts as if it were attached to a stiff spring. The block diagram of the system with this feedback loop is shown in Figure 16. The performance function for this control law is shown in Figure 17 which shows a further increase in the operating region.

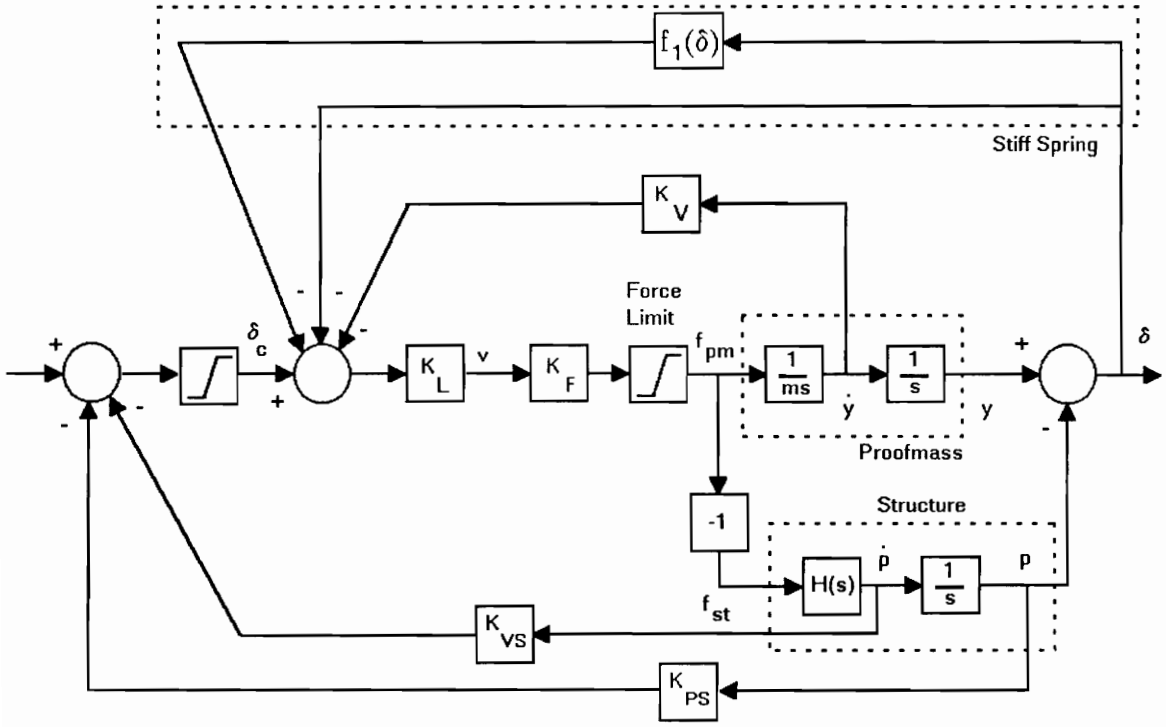

Figure 16. Stiff Spring Control of the Proof-mass

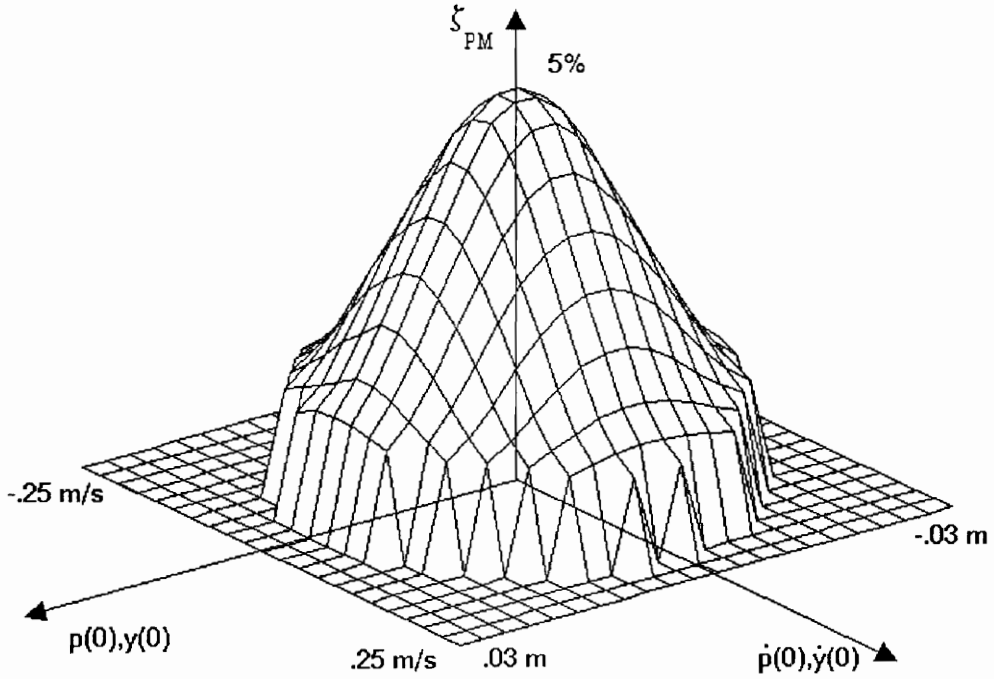

Figure 17. Performance Function using a Stiff Spring Control

Note that the effective damping is significantly degraded near the edges of the operating region. This is an inevitable consequence, since preventing stroke saturation and suppressing vibrations compete for the available force. In fact this division, i.e., how much force is devoted for each objective, is controlled though the gain on the nonlinear function, K_1. In this example (and those that follow), the control gain is adjusted so that the equivalent damping in the nonlinear feedback system equals 5% in the operating region of the linear design. In this way, no performance is sacrificed through the addition of the nonlinear function, which only serves to extend the operating region.

3. Position/Velocity Control

One of the shortcomings of the stiff spring control is its disregard for the velocity of the proof-mass. By monitoring the velocity in addition to the position of the proof-mass, a more effective control can be implemented.

A restoring force is needed only if the proof-mass is predicted to violate its stroke limit. That is, stroke saturation develops only if the position of the proof-mass is near the stroke limit and its velocity is in the direction of increasing displacement. This observation can be incorporated into the nonlinear control law as follows. Define the signum function as:

$$\mathrm{sgn}(x) = \begin{cases} -1, & x < 0 \\ 0, & x = 0 \\ 1, & x > 0 \end{cases} \tag{4.3.1}$$

Now consider the nonlinear feedback function:

$$f_2(\delta,\nu) = \frac{K_2\,\nu}{\left(d - \mathrm{sgn}(\nu)\,\delta\right)^2}, \quad K_2 = 10^{-4} \tag{4.3.2}$$

Where ν is the relative velocity (see (2.3.5)). This function is plotted in Figure 18, and the system block diagram which incorporates this function is shown in Figure 19. The performance function for this control is shown in Figure 20. In this figure, it can be seen that the operating region is increased over the stiff spring control. This control law has shown that performance increases as more information about the state of the proof mass is used.

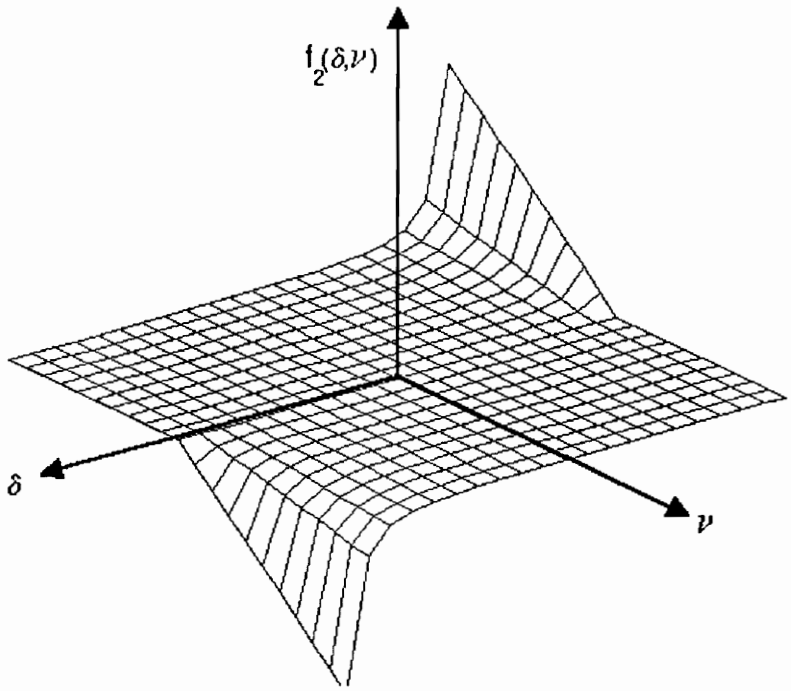

Figure 18. Position/Velocity Nonlinearity

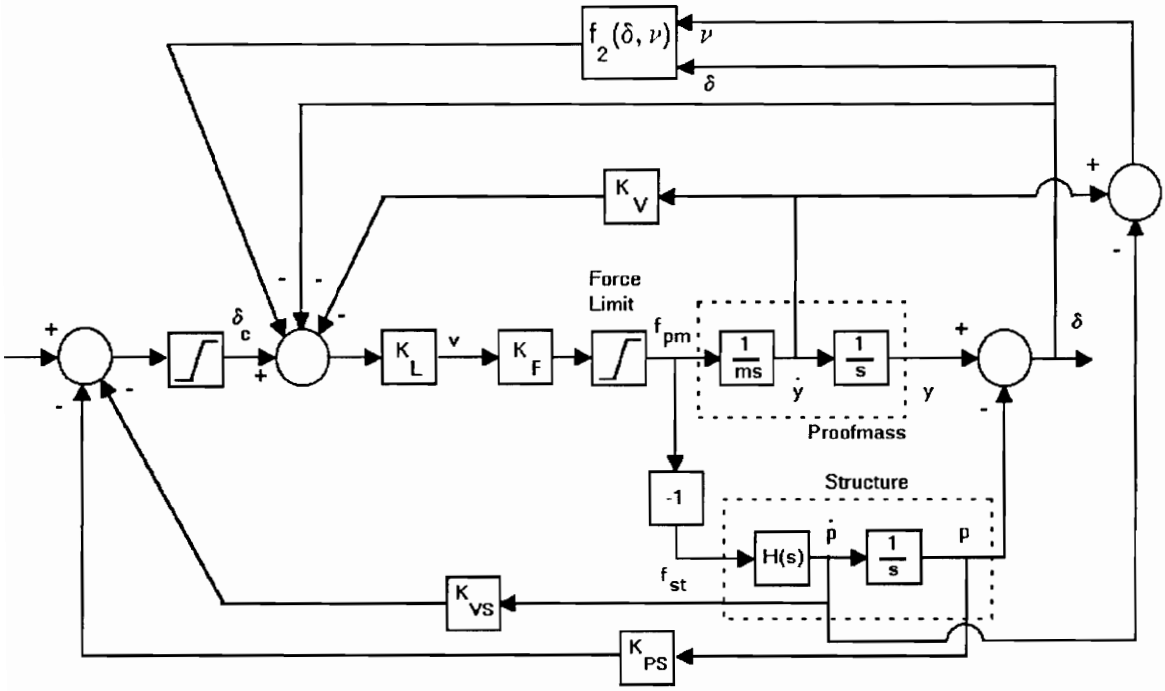

Figure 19. Position/Velocity Nonlinear Control Loops

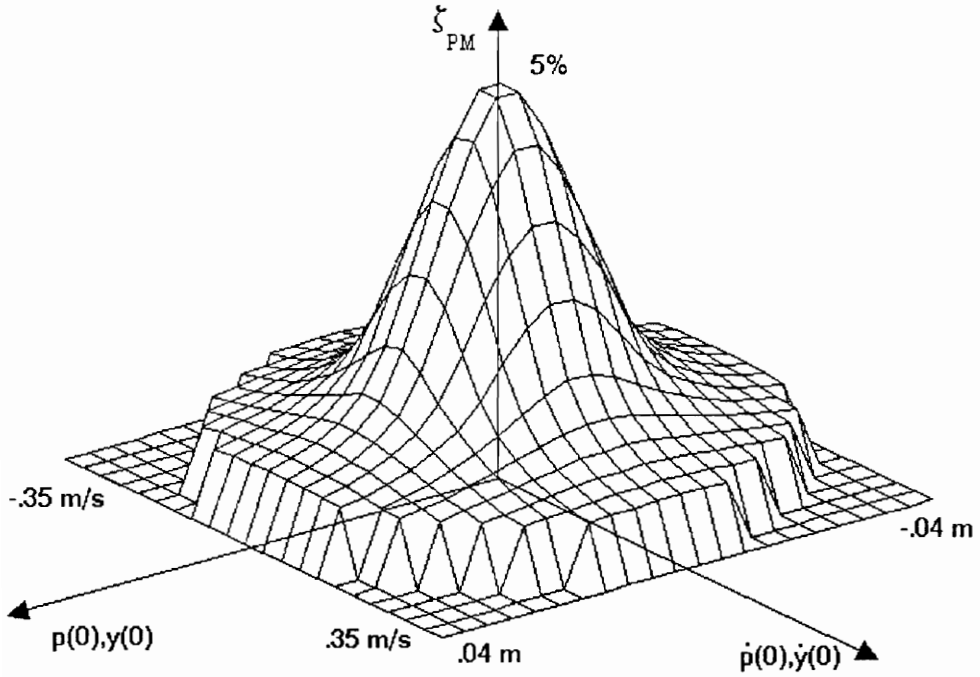

Figure 20. Performance Function for the System using Position/Velocity Control

4. Conclusions

These results can be summarized by comparing the operating regions for the linear control, the linear control with the command limiter, stiff spring control, and the nonlinear control as shown in Figure 21. All of the performance functions have approximately 5% equivalent damping in the operating region of the linear design. Thus, the nonlinear control of the proof-mass serves to extend the operating region over which the proof-mass actuator will not saturate in stroke without decreasing the damping enhancement in the operating region of the linear design.

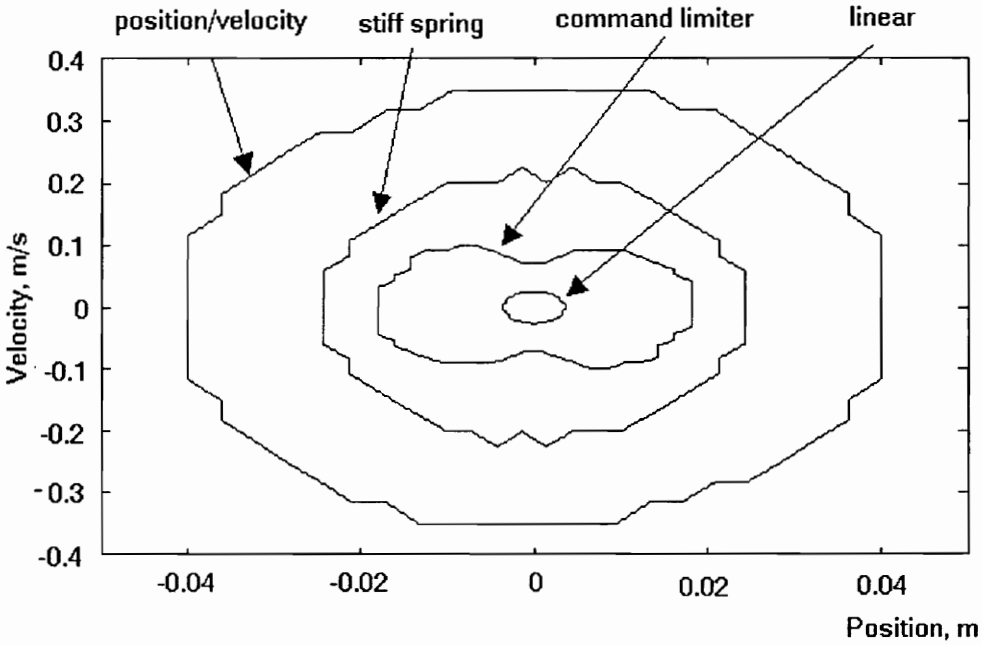

Figure 21. Comparison of Operating Regions with Various Control Laws

CHAPTER 5

EFFECTS OF ACTUATOR PARAMETER VARIATION

In Chapter 4, the performance of a system was evaluated with respect to various nonlinear control laws. In this chapter the performance of the system will be evaluated with respect to a change in actuator parameters. Throughout this chapter, the design techniques developed in Chapter 2 will be applied to actuators with a variety of parameters. Given a particular set of parameters, the control gains of the system are calculated, then the performance of the actuator is evaluated with the damping plot.

As would be expected, there is an inverse relationship between the size of the operating region and the closed loop damping in the structure (assuming the system remains stable). That is, to design the system for larger and larger closed loop damping in the structure would cause the size of the operating region to decrease. This is because the larger the damping requirement the greater the needed force, which increases the likelihood of stroke saturation. Therefore to provide a fair comparison between actuators with various parameters a fixed value of 5% damping is chosen for all systems in this chapter.

1. Variation of Saturation break Frequency

In the design of the vibration suppression loops, the relationship between the modal frequency of the structure, ω_S, and the saturation break frequency, ω_B, is of

crucial importance as is discussed in Chapter 2. By varying ω_B, which is determined by the parameters of the actuator (See (2.2.3)), the performance of various size actuators can be investigated for a given structure. The saturation break frequency can be altered by changing the F_{Max}, d, or m. If F_{Max} is increased while d and m are held constant, the performance of the actuator will certainly increase also. This is because if F_{Max} is larger, the force will saturate less often, which means the stroke will saturate less often. Likewise, if d is increased while F_{Max} and m are held constant, there will be less stroke saturation and thus the operating region will be larger. Therefore it would be difficult to compare two actuators with a different maximum force or stroke.

To provide an equal comparison, all actuators discussed in this section will have a fixed maximum force at F_{Max} = 30N and a fixed stroke length at d = 0.15m. Three cases are considered for three different choices of the mass of the proof-mass. The system considered in this section contains only the force saturation nonlinearity and does not contain any nonlinear control. The structure of the system is shown in Figure 6 and the design was carried out as described in Chapter 2. The parameter values along with the corresponding values of the saturation break frequency and the gains for the linear loops are shown in Table 5.

Table 5. Linear Control Loop Gains

	K_V	$K_L K_F$	K_{ps}	K_{vs}	ω_B (Rad/s)
m = 1 kg	0.09810	200	0	26	14.142
m = 10 kg	0.31305	200	0	-11.5	4.472
m = 3 kg	0.17146	200	-69.8	0	8.165

Case 1: m = 1 kg

From (2.2.3) this size of proof-mass results in $\omega_B >> \omega_s$. From the stroke/force saturation curve (Figure 3), this relationship results in limited force availability for vibration suppression due to the stroke limit. Assuming that all of that force is used, the actuator will tend to saturate in stroke, reducing the operating region. The performance function for this system is shown in Figure 22. Note that, as expected, the operating region is very small.

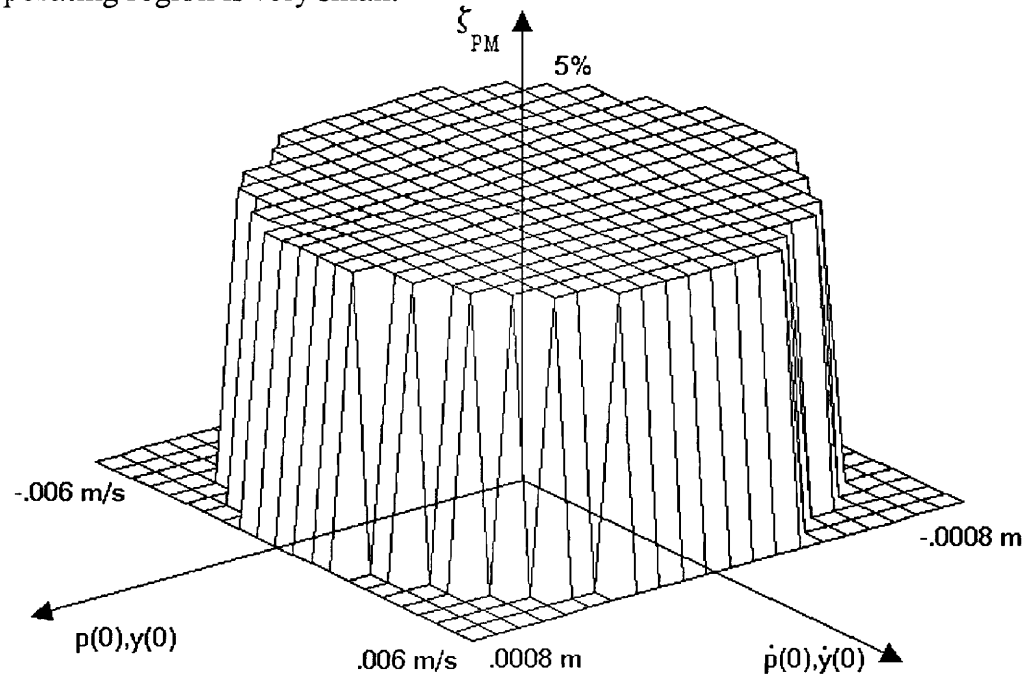

Figure 22. Performance Function for m = 1 kg

Case 2: m = 10 kg

This size of proof-mass results in $\omega_B << \omega_s$. In this regime, it can be seen from the stroke/force saturation curve that stroke saturation will occur only after force saturation occurs. Therefore the force limit functions to control stroke saturation. Figure 23 shows the performance function for the system discussed here. Note that

the operating region has been expanded, but that poor performance is observed near the boundary of the operating region due to the action of the force limit.

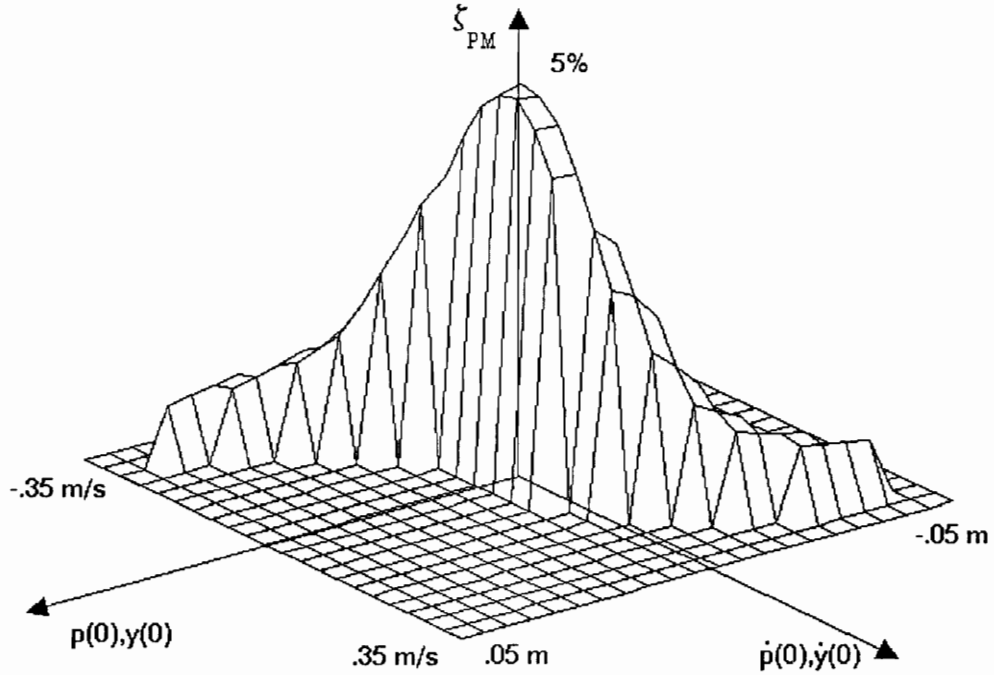

Figure 23. Performance Function for m = 10 kg

Case 3: m = 3 kg

When the system is configured such that $\omega_B << \omega_s$, as in Case 2, the stroke saturation curve is above the force saturation curve implying that the mass of the proof-mass is not being optimally utilized. In Case 1 with $\omega_B >> \omega_s$ it was found that the operating region was prohibitively small. This is because in order to use all of the force available, the actuator must saturate in stroke. This observation suggests that the actuator should be sized such that the saturation break frequency, ω_B, should be approximately the same as the structure's modal frequency, ω_s:

$$\omega_s \approx \omega_B = \sqrt{\frac{F_{Max}}{m\,d}} \tag{5.1.1}$$

With this configuration of parameters, the full force, limited by the stroke and force saturation, is used by the actuator. When m = 3 kg the parameters of the system considered here have this relationship. The performance function for this set of parameters is shown in Figure 13.

The operating regions of these three actuators are shown in Figure 24. The operating region for the 10 kg mass is increased over the 3 kg mass because the excess stroke in Case 2 was used to absorb transients in the relative position. Since the stroke is used to its full potential in Case 3, the it is now apparent that the proof-mass actuator can be used to its full capacity if the parameters are selected to match the structure's frequency as in Case 3 and the nonlinear control techniques derived in Chapter 4 are applied to the system to prevent the transients from violating the stroke limit.

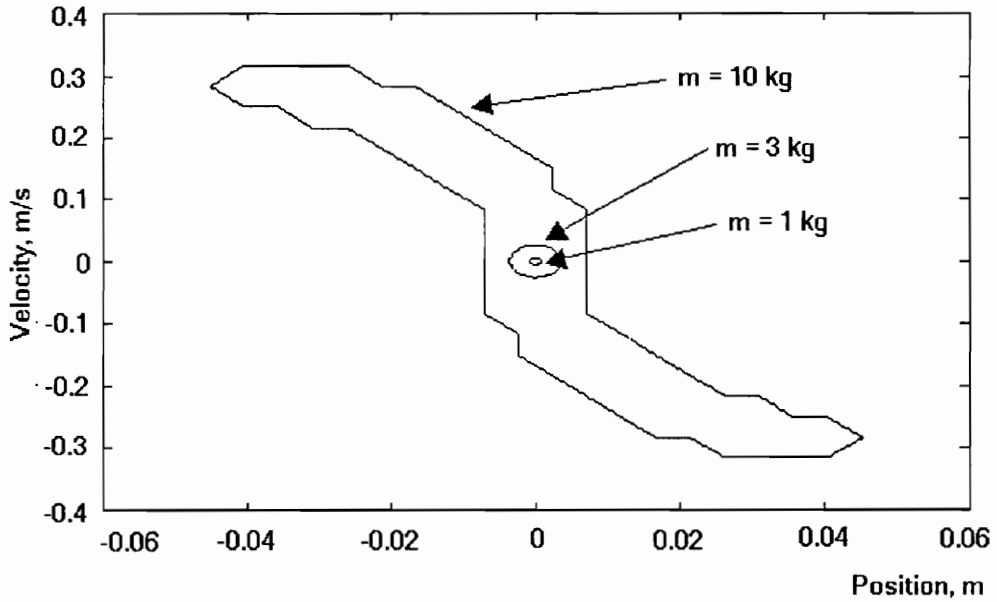

Figure 24. Comparison of Operating Regions for Different Saturation break Frequencies

In Figure 25, the operating regions of the actuator with the 3 kg proof-mass with position/velocity nonlinear control is compared to the operating region of the actuator with a 10 kg proof-mass with linear control. As can be seen from this comparison, the operating region with the 3 kg mass is equal, if not larger, than the operating region with the 10 kg mass. This result implies that the same level of damping enhancement in the structure with a larger operating region can be obtained from an actuator with smaller proof-mass through the use of nonlinear control. In summary, the actuator should be designed such that the saturation break frequency equals the modal frequency of the structure. To prevent the transients from violating the stroke limit, some type of nonlinear control scheme should be applied.

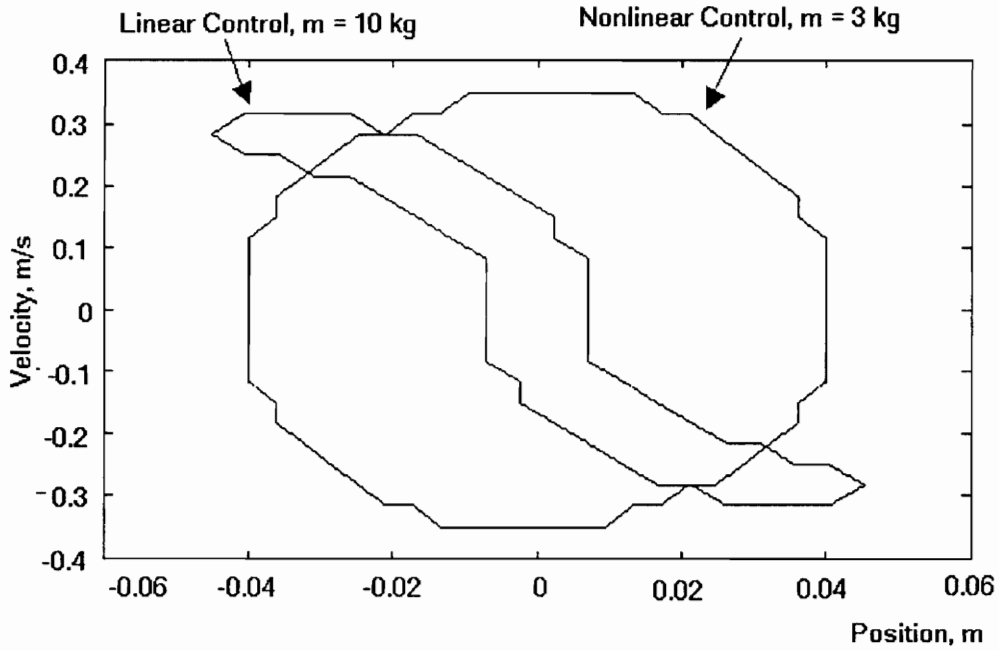

Figure 25. Comparison of Operating Regions for Linear and Nonlinear Control

Consider the case when the structure contains more than one mode. How should these principles be applied here? Surely, if any lightly damped modes are lower than the saturation break frequency, their amplitudes will dominate the relative position and cause stroke saturation similar to Case 1 above. On the other hand, as was shown for Case 2, responses from modes with frequency above the saturation break frequency are controlled through the action of the force limit. For these reasons, the saturation break frequency should be designed to match the lowest modal frequency of the structure. As for the performance, the operating region of a multi-modal structure system would be expected to be smaller than a single mode system since the available force for vibration suppression must be divided among the modes.

2. Variation of Proof-mass Mass

The analysis in the last section suggested that to use the actuator to its full capacity, the mass, m, the stroke length, d, and the maximum available force F_{Max}, should be chosen such that the saturation break frequency is approximately the same as the frequency of the mode to be controlled; i.e.:

$$\omega_s \approx \omega_B = \sqrt{\frac{F_{Max}}{m\,d}} \tag{5.1.1}$$

This relationship specifies the relationship between F_{Max} and the product, md, but it does not uniquely determine the mass or the stroke. In this section the effect of changing the mass and stroke, subject to (5.1.1), on the performance of the actuator is investigated.

In this section three different actuators are considered on the same structure used in the last section.

Case 1: m = 3 kg and d = 0.15 m

Case 2: m = 1 kg and d = 0.45 m

Case 3: m = 10 kg and d = 0.045 m

Note that in all cases the product md is constant and each satisfy (5.1.1). The design techniques developed in Chapter 2 are applied to each case. These control gains and parameters are shown in Table 6.

Table 6. System Parameters for Actuators with Constant md

	Case 1	Case 2	Case 3
Actuator Parameters:			
m (kg)	3	1	10
d (m)	0.15	0.45	.045
Fmax (N)	30	30	30
Actuator Control Gains			
$K_L K_F$	200	66.67	666.67
K_V	.17146	.17146	.17146
Vibration Control Gains			
K_{ps}	-69.8	-211.2	-20.22
K_{vs}	0	0	0
Nonlinear Control Gains			
K1	2×10^{-4}	0.005	5×10^{-5}
K_2	10^{-4}	0.001	10^{-5}

First, consider these three actuators when only linear control loops are used. The performance function for Case 1 is shown in Figure 13. The performance function for Case 2 and Case 3 are shown in Figures 26 and 27 respectively. These three plots are almost identical. Evidently, trading off mass against stroke has very little effect on the performance of proof-mass actuators with only linear control loops.

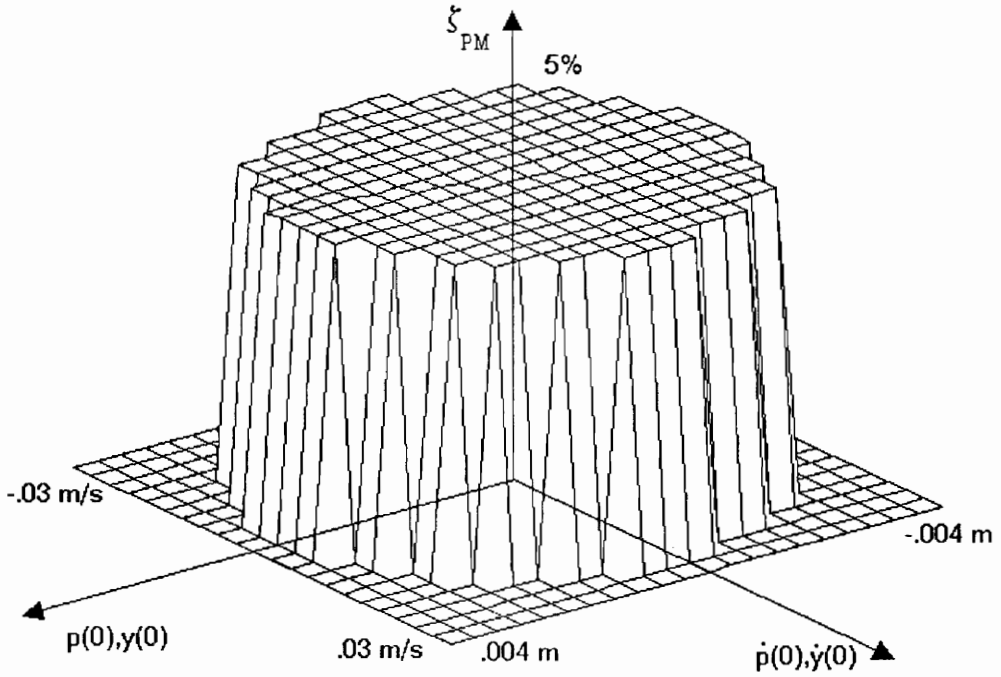

Figure 26. Performance Function for 1 kg Mass and 0.45 Stroke

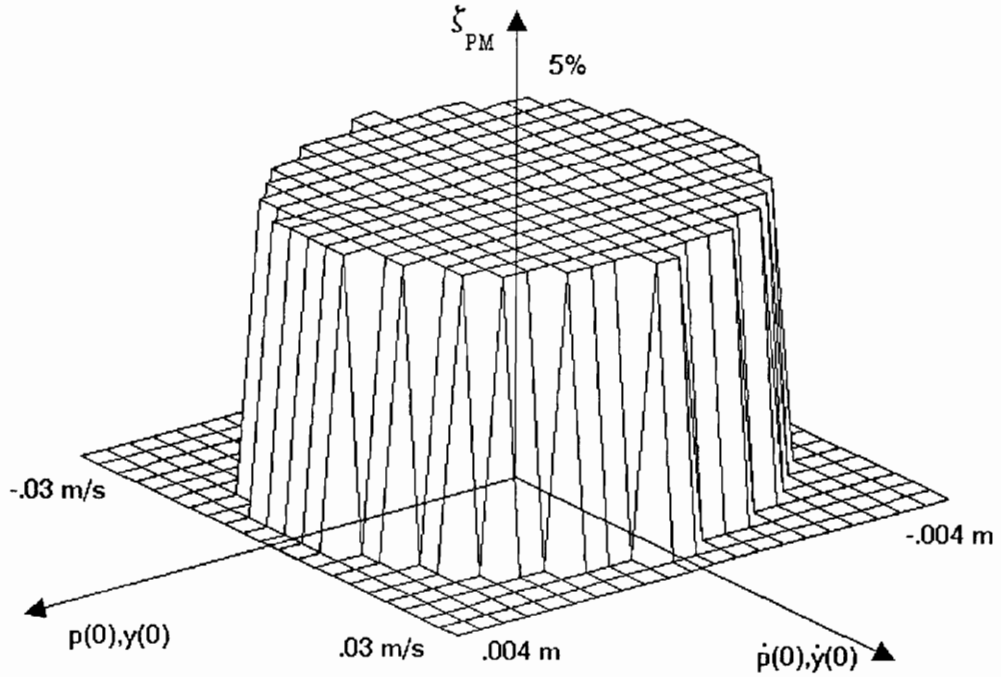

Figure 27. Performance Function for 10 kg Mass and 0.045 m Stroke

Next consider these three cases when the actuators have the nonlinear control loops discussed in Chapter 4. In each case the nonlinear feedback functions are adjusted to the stroke length as necessary. Also, the nonlinear function gains are adjusted such that the equivalent damping is the same in the operating region of the linear design. These gains are shown in Table 6.

First, the command limiter is added to the vibration suppression loop for each case. The limit on each saturation function was set to the corresponding stroke length. The performance function for the 3 kg case is shown in Figure 15. The performance functions for the other two cases are shown below in Figures 28 and Figure 29.

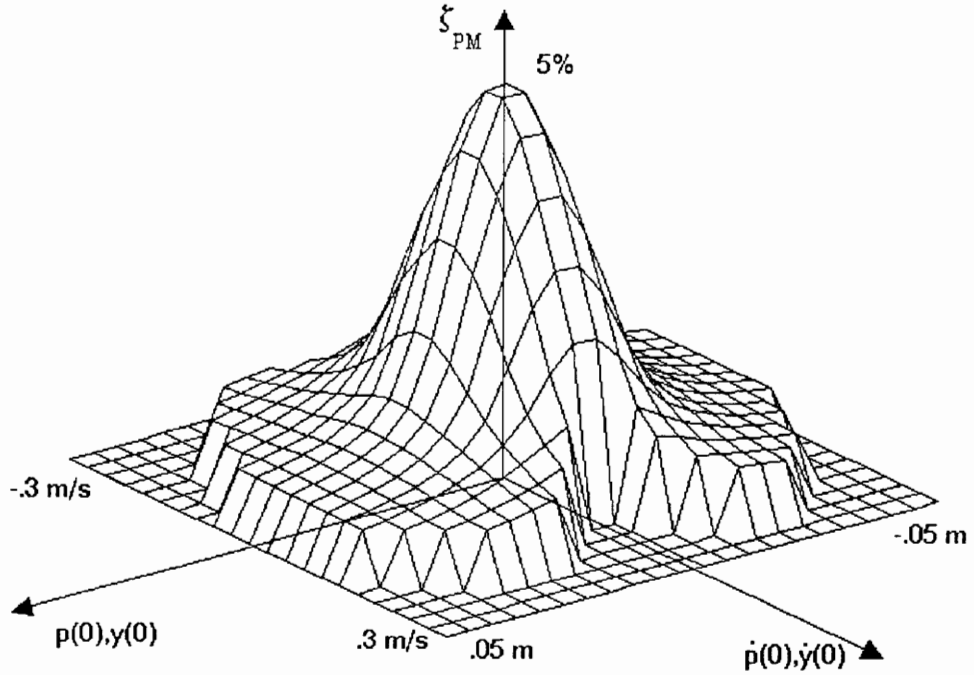

Figure 28. Performance Function for 1 kg Mass and 0.45 m Stroke with Command Limit

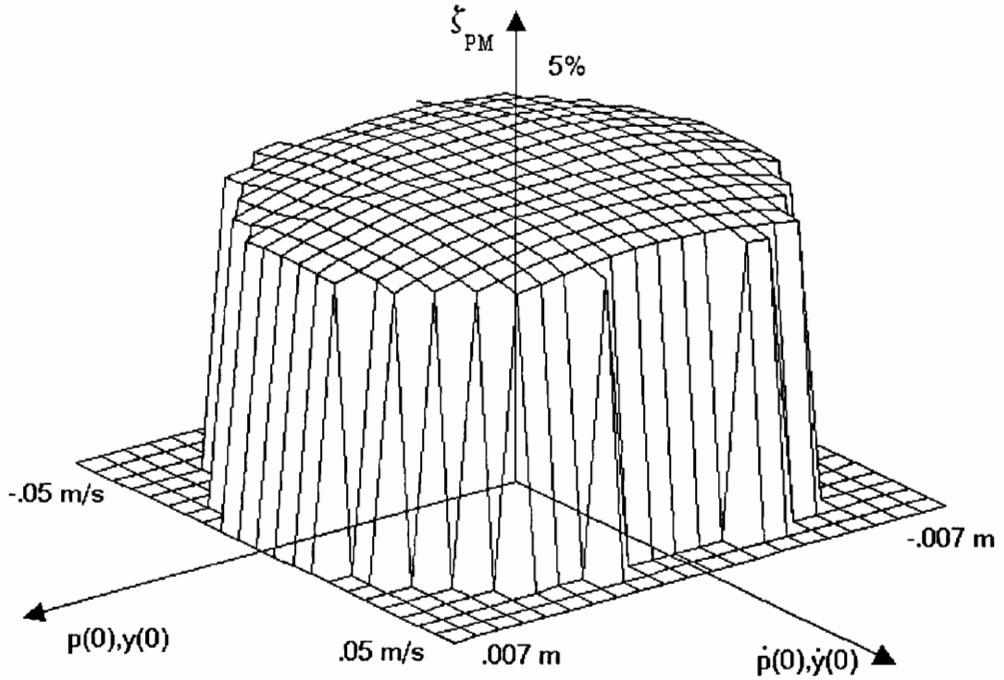

Figure 29. Performance Function for 10 kg Mass and 0.045 m Stroke with Command Limit

Next the actuator control loops are augmented with a stiff spring and the position/velocity nonlinearity as discussed in Chapter 4. The performance functions for a 3 kg mass are shown in Figure 17 and Figure 20. The performance functions for the other cases are shown below in Figures 30-33.

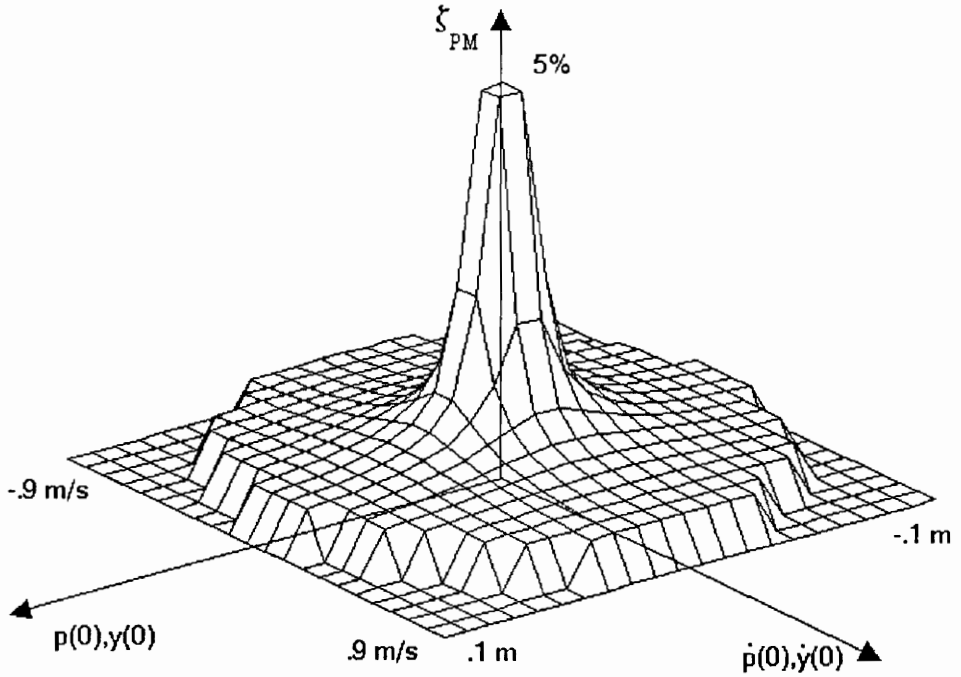

Figure 30. Performance Function for 1 kg Mass and 0.45 m Stroke with Stiff Spring

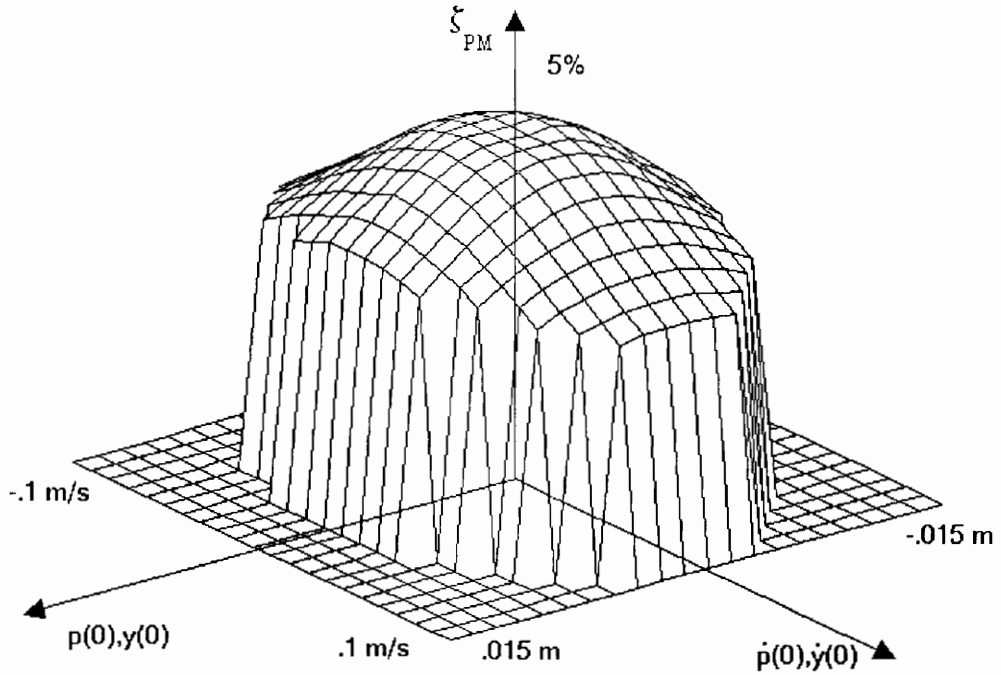

Figure 31. Performance Function for 10 kg Mass and 0.045 m Stroke with Stiff Spring

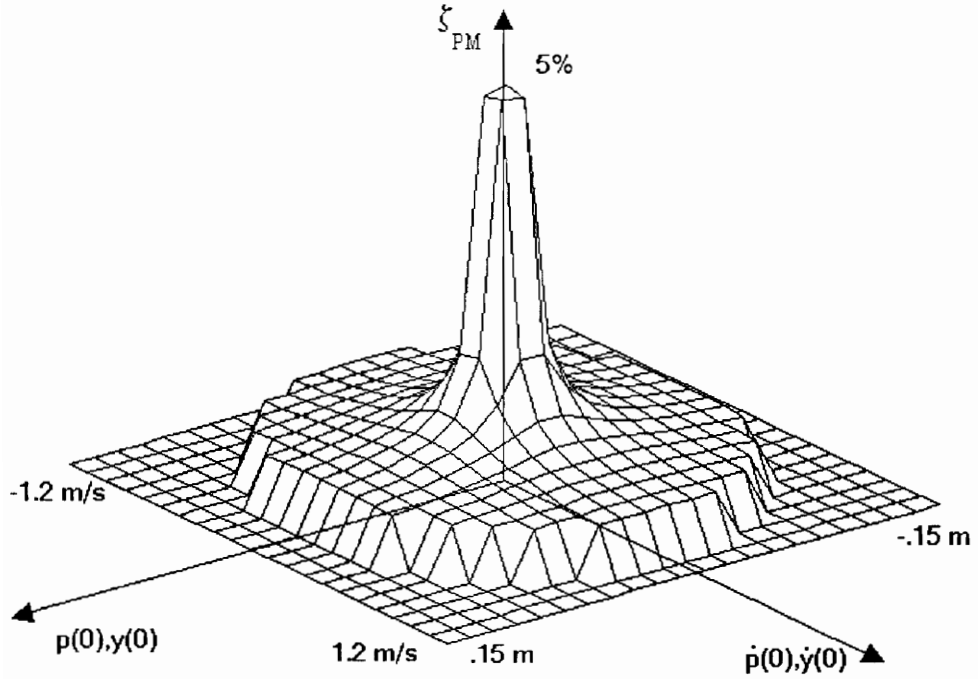

Figure 32. Performance Function for 1 kg Mass and 0.45 m Stroke with Position/Velocity Nonlinearity

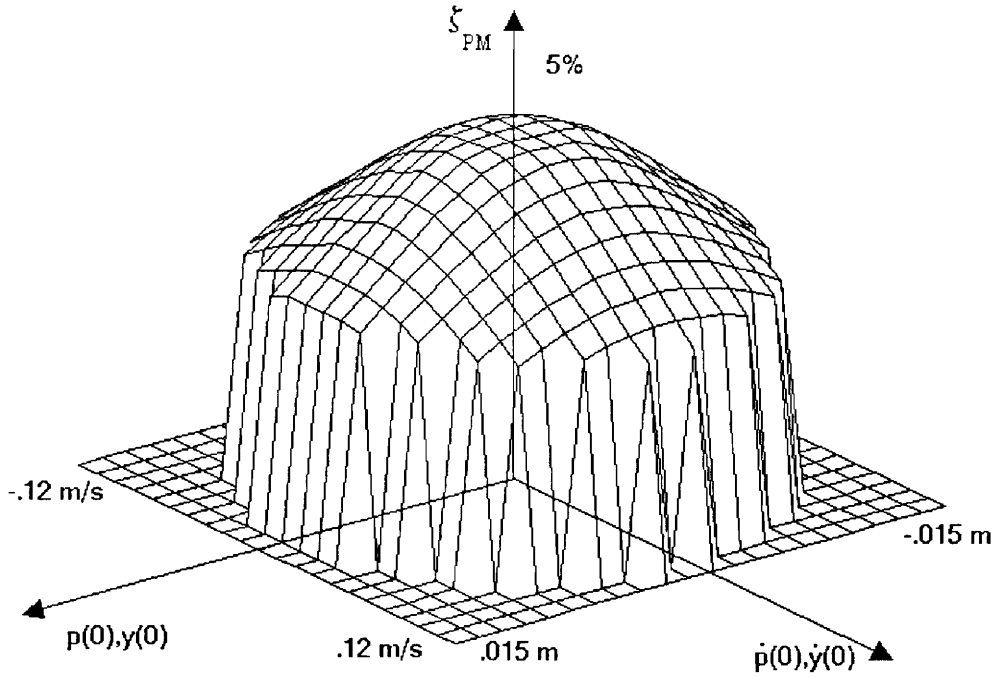

Figure 33. Performance Function for 10 kg Mass and 0.045 m Stroke with Command Limit and Position/Velocity Nonlinearity

The operating regions for each of the actuators discused above are shown in Figure 21 and Figures 34 and 35 below. As was shown in Chapter 4, in each case the operating region is increased by the addition of the nonlinear control loops.

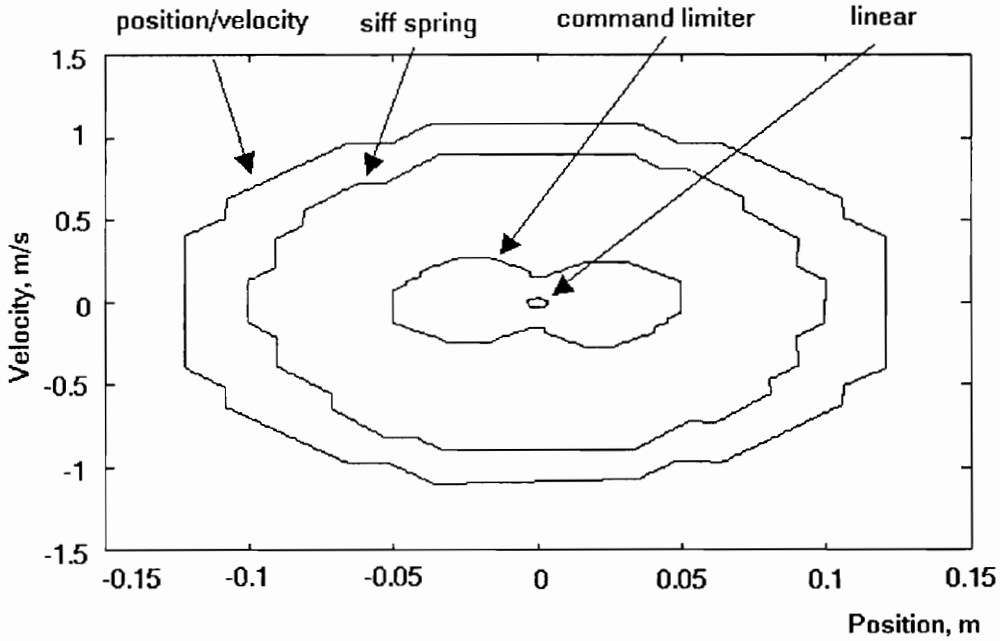

Figure 34. Comparison of Operating Regions for m = 1 kg and d = .45 m

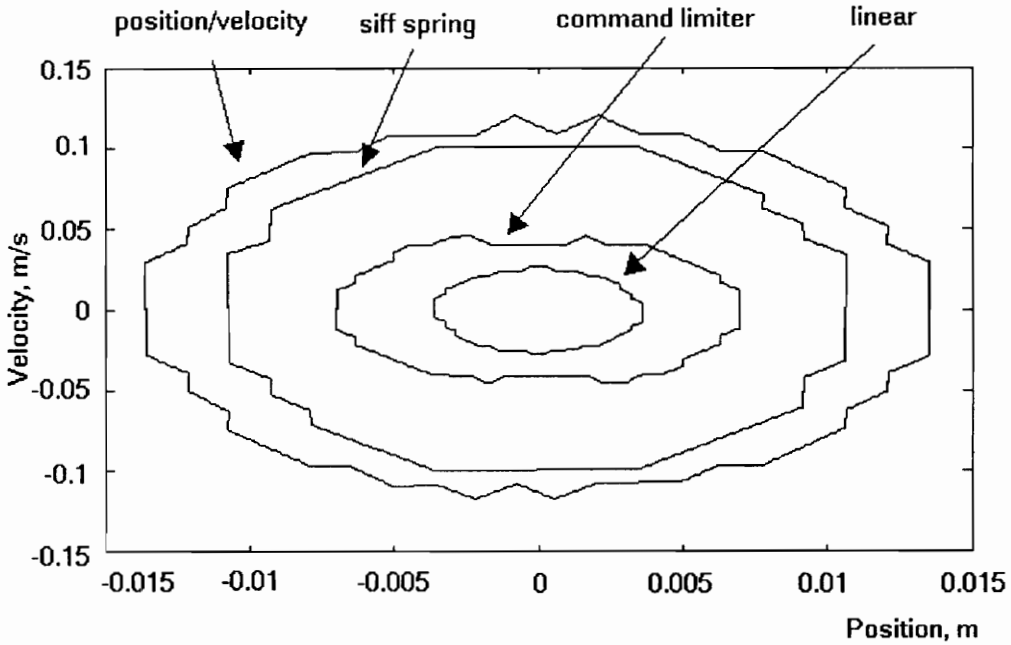

Figure 35. Comparison of Operating Regions for m = 10 kg and d = .045 m

A comparison between the operating regions of the three actuators, each with the same mass/stroke products but with different mass is shown in Figure 36. This

plot compares the systems with the nonlinear position/velocity control. This figure shows a clear trend of increasing operating region as the stroke of the actuator increases and the mass decreases. It is important to note that the differences due to changing the mass only appear in the systems with nonlinear control. This can be seen by comparing Figures 13, 26, and 27, which show that the operating region does not change for different parameters (mass and stroke) when the product md is kept constant. In conclusion, it can be said that the larger the stroke of the actuator, the better the performance of the actuator. Not only does the size of the operating region increase with stroke length, but for a given structure, the larger the stroke length, the lighter the proof-mass. This is an important result since in most applications the "dead-weight", or the mass not associated with the structure, should be minimized.

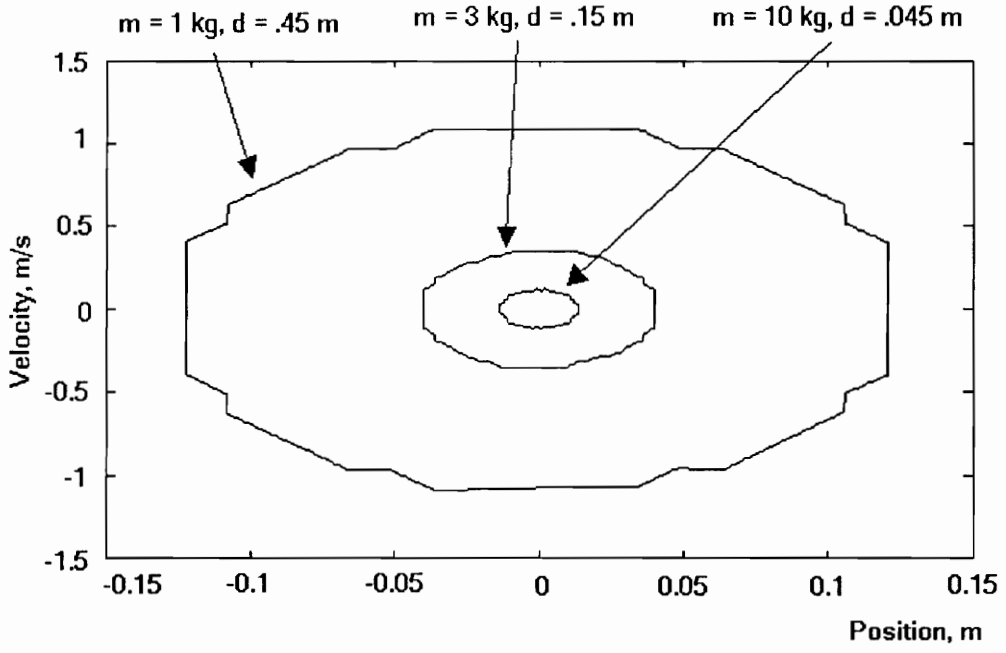

Figure 36. Comparison of Operating Regions with Position/Velocity Nonlinearity

CHAPTER 6

LIMIT CYCLE ANALYSIS

The nonlinear control proposed in Chapter 4 shows a definite improvement in the performance of the proof-mass actuator. In this chapter the possible presence of limit cycles is investigated. In the first section, the system is analyzed without the nonlinear feedback control. In this case the system has a single nonlinearity, the force limit, which lends itself to describing function analysis. Due to the simplicity of this system, this analysis finds a relation of parameters that precludes the existence of limit cycles even with the inclusion of an arbitrary multimodal structure. In the sections that follow, the effects of the nonlinear control is investigated. Because of the multiple nonlinearities in these systems, a different type of analysis is employed. This technique is based on the concept of harmonic balance which assumes a sinusoidal limit cycle, but does not approximate the nonlinearities as in describing function analysis. These sections conclude that the control nonlinearities presented here do not make the system more susceptible to limit cycles.

1. Describing Function Analysis

In this section describing function analysis will be applied to the system with only the force saturation. A describing function replaces a nonlinearity with a function that relates the amplitude and phase of an input sinusoid to an output amplitude and phase of the fundamental harmonic. It is assumed that the input into

the nonlinearity is sinusoidal and contains only the fundamental harmonic, which implies that the closed loop system must be essentially a low pass filter to attenuate any higher harmonics. Frequency domain analysis is then applied to the system to determine if any amplitudes cause a sustained oscillation. This is characterized by the condition of a negative unity loop gain.

Consider the block diagram of the system in Figure 37. Note that the structure is not limited to a single mode structure. Here the force saturation nonlinearity is replaced by its describing function, N(a) (Atherton, 1982):

$$N(a) = \begin{cases} 1, & a \leq F_{Max} \\ (1/\pi)(2\alpha + \sin 2\alpha), & a > F_{Max} \end{cases} \qquad (6.1.1)$$

where $\alpha = \sin^{-1}(F_{Max}/a)$, a is the amplitude of the input signal to the force saturation, and F_{max} is the force limit.

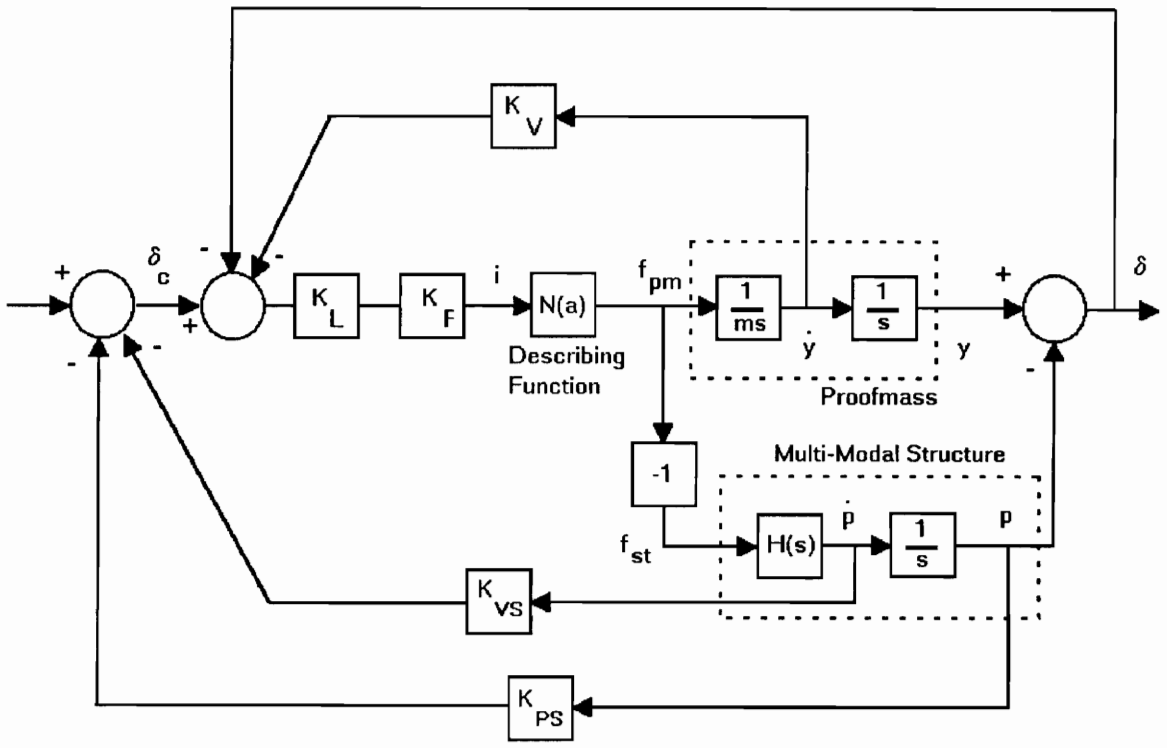

Figure 37 Block Diagram of the System with Structure and Compensator

Assume that a sinusoidal limit cycle exists in the system entering the nonlinearity such that:

$$i(t) = a_0 \sin \omega_0 t \tag{6.1.2}$$

Describing function analysis predicts a limit cycle if:

$$1 + \mathrm{N}(a_0)\frac{i(j\omega_0)}{\mathrm{f_{pm}}(j\omega_0)} = 0 \tag{6.1.3}$$

Through simple block diagram manipulation, the system in Figure 37 can be reduced to the system in Figure 38.

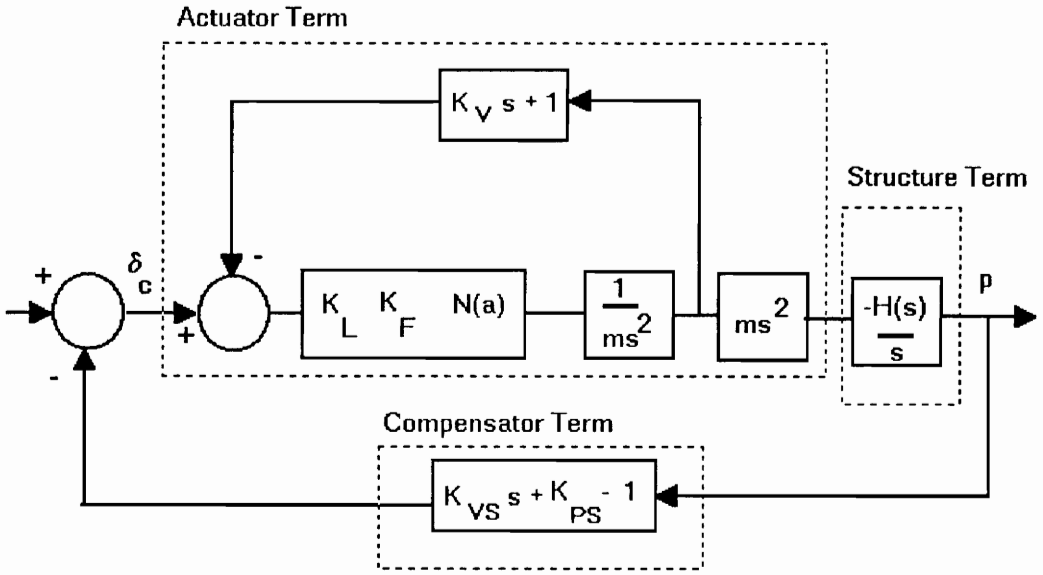

Figure 38 Block Diagram of the Reduced System

Thus from the form of the system in Figure 38, (6.1.3) is equivalent to:

$$A(j\omega_0)\, C(j\omega_0)\, \frac{-H(j\omega_0)}{j\omega_0} = -1 \tag{6.1.4}$$

where:

$$A(s) = \left(\frac{K_L K_F\, N(a_0)\, m\, (j\omega_0)^2}{m\, (j\omega_0)^2 + K_V K_L K_F\, N(a_0)\, (j\omega_0) + K_L K_F\, N(a_0)} \right)$$

$$C(s) = \left(K_{vs}\, (j\omega_0) + K_{ps} - 1 \right) \tag{6.1.5}$$

Consider the phase of the left hand side of (6.1.4). The first product, A(s), is called here the "actuator term", the second product,C(s), is called here the "compensator term" and the last product is called here the "structure term." These three terms are derived from separate sections of the block diagram and are marked in Figure 38. Note that the phase of these terms can be studied separately and if the

sum of the phase of these terms is between -180 and 180 degrees for all frequencies, no limit cycle will be possible.

The actuator term represents the effect of the actuator in the system. The phase of this term depends on the input amplitude to the nonlinearity, a_0. When this amplitude is less than F_{max}, $N(a_0)$ equals one and the phase of this term will be similar to Figure 39. When a_0 exceeds the saturation level F_{max} the value of $N(a_0)$ is between zero and one. As the amplitude of signal a grows large, N(a) approaches zero. The variation of the function N(a) merely reduces the break frequency of this expression. And as the amplitude grows larger and larger, the phase of this term approaches zero for all frequencies. Therefore the phase of the actuator term could be anywhere in the region shown in Figure 40.

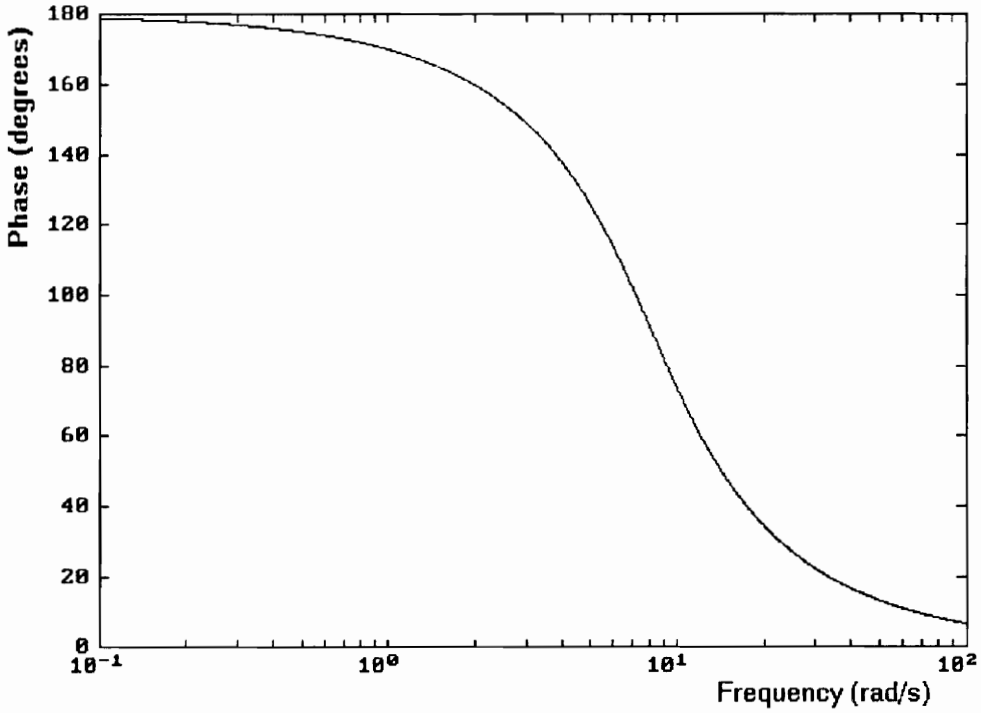

Figure 39 Phase of Actuator Term for Low Amplitudes

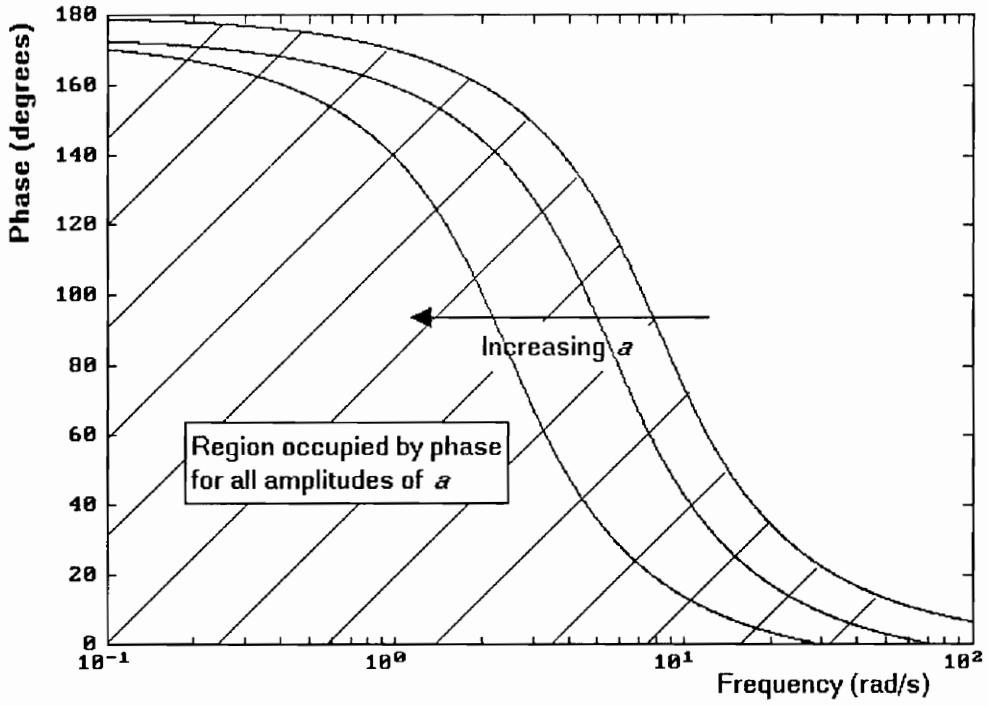

Figure 40 Region Occupied by Phase of Actuator Term

The compensator term represents the effect of the vibration suppression loops. In fact, the compensator term is very similar to the compensator term (2.4.1) used for the phase compensation arguments. The question that now needs to be answered is that if phase compensation is used as described in Chapter 2, can the system experience limit cycles?

Notice that the phase of the structure term for an arbitrary structure with co-located actuator and sensor is between 0 and 180 degrees. Therefore the sum of the phase of the compensator term and the actuator term must be between -180 degrees and 0 for all frequencies. With this bound and the observation from Figure 40, a bound for the phase of the compensator term can now be determined. From (6.1.4):

$$-180^{\circ} \leq \arg(C(s)) \leq -\sup\{\arg(A(s))\} \tag{6.1.6}$$

That is, the phase of the compensator must be between -180 degrees and the negative of phase shown in Figure 39. This limits the phase of the compensator to be around -180 degrees for low frequencies. Figure 41 illustrates this region.

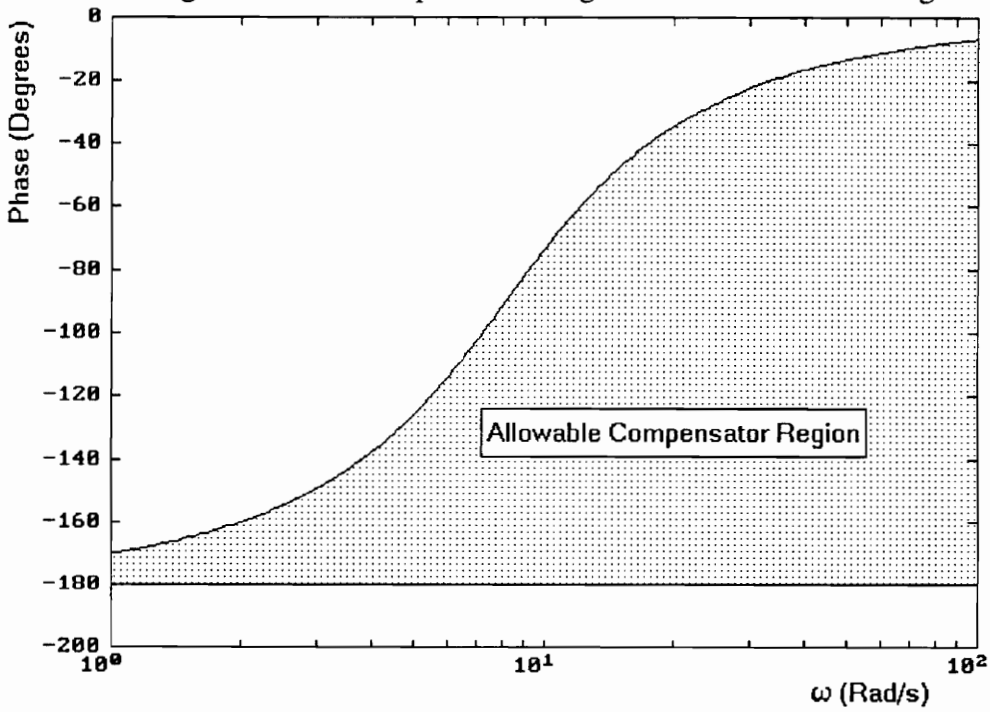

Figure 41 Allowable Compensator Region

Since the phase of the compensator is restricted by changing K_{vs} and K_{ps} in C(s), a bound for these parameters is found by writing an explicit expression for the phase of C(s) and comparing it to the phase of A(s). Thus following inequality is derived from (6.1.6):

$$K_V(K_{ps} - 1) \leq K_{vs} \leq 0 \tag{6.3.7}$$

Since K_V is related to the saturation break frequency by (2.2.6), the following is true: if the zero of the compensator term, $(K_{ps}-1)/K_{vs}$, is significantly larger then the saturation break frequency, ω_B, then the phase of the left hand side of (6.1.4) will never be -180 degrees for any structure and (6.1.4) will never be satisfied.

If this rule is violated, then the phase may equal -180 for some frequency, ω, and amplitude, a. If the magnitude of the left hand side of (6.1.4) also equals unity at this point, a limit cycle would be predicted by this describing function analysis. Consider the cases when this is possible. If the structure is has only a single mode and the phase compensation guidelines are followed from Chapter 2, a limit cycle can appear if the structure's modal frequency is not close to ω_B. This is because the choice of K_{vs} and K_{ps} for Type 1 and Type 3 relations from Chapter 2, would obviously violate (6.3.7) because of their signs. It should be noted that limit cycles in these cases exists in pairs: one stable and one unstable (Atherton, 1982). If an initial condition is smaller than the unstable limit cycle, then the system will converge asymptotically to the origin. Otherwise the system will move into the limit cycle.

For a multimodal structure, it was argued in Chapter 2, that only the modes equal to and greater than ω_B can have their damping increased with the structure of Figure 6. When phase compensation is applied in this case, the phase of modes equal to and greater than the break frequency must be adjusted to depart at -180 degrees. This is done by choosing the gains K_{vs} and K_{ps} to be negative and the ratio K_{ps}/K_{vs} to be significantly larger than ω_B. These requirements will naturally satisfy (6.3.7).

In conclusion, for a single mode structure, the actuator should be designed so that the saturation break frequency is approximately equal to the structure's modal frequency to prevent limit cycles caused by the force saturation. For a multi-modal structure, the actuator is designed to match the lowest modal frequency. Then, when phase compensation is applied, the damping of the modes will increase while simultaneously avoiding limit cycles caused by the force saturation nonlinearity.

2. Harmonic Balance

Now that the system is understood with only the force saturation, consider the system in Figure 19 with the nonlinear feedback (4.3.2). Due to the presence of multiple nonlinearities, harmonic analysis will be employed to investigate the existence of limit cycles. To that end assume that the relative position exhibits a sustained sinusoidal oscillation:

$$\delta(t) = A\cos(\omega t) \tag{6.2.1}$$

Because of the finite stroke length, only $0 \le A \le d$ needs to be considered. From Figure 19, the force applied to the proof-mass, f_{pm}, is related to the relative position by:

$$\frac{\delta(s)}{f_{pm}(s)} = \frac{1}{m s^2} + \frac{H(s)}{s} \tag{6.2.2}$$

If (6.2.1) holds, then $f_{pm}(t)$ is sinusoidal and its magnitude and phase are the magnitude and phase of the complex number:

$$\frac{A}{\frac{1}{m(j\omega)^2} + \frac{H(j\omega)}{j\omega}} \tag{6.2.3}$$

Similarly, the magnitude and phase of $y(t)$, $\dot{y}(t)$, $p(t)$, and $\dot{p}(t)$ can also be computed. These signals, which are periodic, provide the input into the nonlinearities of the system. The input into the force saturation, $v(t)$, is periodic and is represented by:

$$V(\theta) = K_L\Big[- K_V\dot{Y}(\theta) - \Delta(\theta) - f_2\big(\Delta(\theta),\dot{\Delta}(\theta)\big) + S_{\delta_{cmax}}\Big(- K_{ps}P(\theta) - K_{vs}\dot{P}(\theta)\Big)\Big] \tag{6.2.4}$$

where:

$$\begin{aligned}
\Delta(\theta) &= A \cos\theta, \\
\dot{\Delta}(\theta) &= -A\,\omega \sin(\theta), \\
\dot{Y}(\theta) &= |\dot{y}| \cos(\theta + \angle\dot{y}), \\
P(\theta) &= |p| \cos(\theta + \angle p), \text{ and,} \\
\dot{P}(\theta) &= |\dot{p}| \cos(\theta + \angle \dot{p}).
\end{aligned} \tag{6.2.5}$$

Where, for example, $|p|$ represents the magnitude of the sinusoidal oscillation of p(t). Therefore, the output of the force saturation will be periodic. Decomposing this signal into its Fourier series, the fundamental amplitude and phase are given by the amplitude and phase of:

$$f_c(A,\omega) = \frac{1}{\pi}\int_0^{2\pi} e^{-j\theta}\, S_{F_{max}}(K_v\, V(\theta))\, d\theta \tag{6.2.6}$$

Harmonic balance predicts a limit cycle if

$$f_c(A,\omega) = \frac{A}{\dfrac{1}{m\,(j\omega)^2} + \dfrac{H(j\omega)}{j\omega}} \tag{6.2.7}$$

or,

$$\left[\frac{1}{m\,(j\omega)^2} + \frac{H(j\omega)}{j\omega}\right]\frac{-f_c(A,\omega)}{A} = -1 \tag{6.2.8}$$

A Nyquist-like plot of the left side of (6.2.8) can be generated. If this curve passes through -1 + j0, a limit cycle at that amplitude and frequency is predicted. This plot will be considered a Nyquist plot in this chapter. A flow chart of the algorithm that generates the Nyquist chart is included in the Appendix.

3. Analysis of the Effect of Nonlinear Control

Using the harmonic balance analysis in the last section, it can be determined if the various nonlinearities cause limit cycles. In this section, the parameters for the system will be identical to the system used Chapter 4.

First, consider the system with only linear control loops and command limiter shown in Figure 14. Figure 42 shows a Nyquist plot with δ_{cmax} = 0.15 m. Clearly, this plot is bounded away from the -1 point, so no limit cycle is predicted. Of course, this analysis would have to be repeated for each A, $0 \leq A \leq d$. It can be shown that the Nyquist curve in Figure 42 moves away from the critical point as A is decreased. It can be concluded that no limit cycle exists for this selection of control gains.

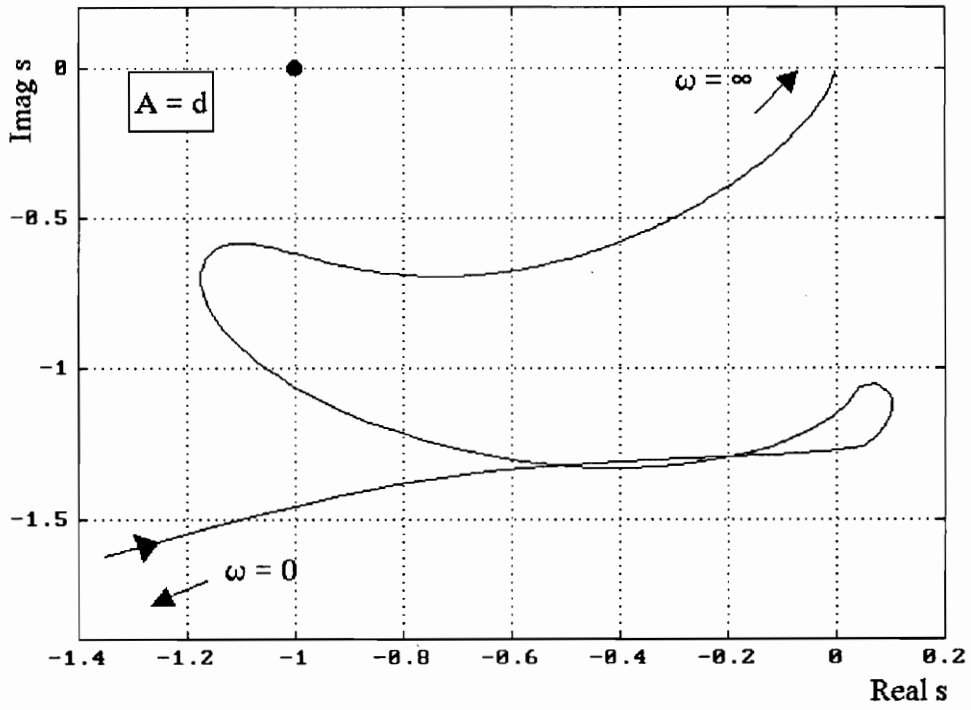

Figure 42 Nyquist Plot of System with Command Limit

The effect the command limiter has on the Nyquist plot can be determined by plotting several Nyquist plots with different values of δ_{cmax}. Figure 43 shows several Nyquist plots with δ_{cmax} equal to 0.20 m, 0.10 m and the extreme case of 0 m, which is actually an open loop system. As can be seen by this graph, as δ_{cmax} decreases the Nyquist graph moves toward the open loop system (no vibration suppression loops). Thus, since the system is not conditionally stable as the vibration suppression gains

go to zero (i.e. the root locus does not cross the $j\omega$ axis), the command limiter cannot cause a limit cycle.

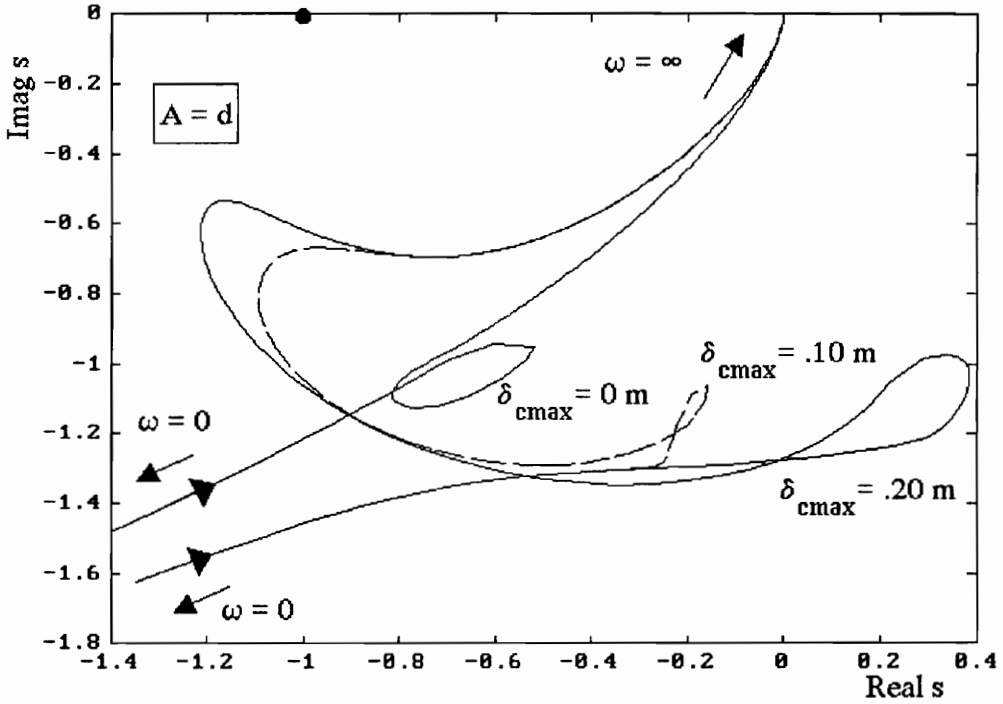

Figure 43 Nyquist Plots Showing the Effect of the Command Limiter

Continuing on with this analysis a stiff spring function is added to the system for stroke saturation control as shown in Figure 16. In this system δ_{cmax} has a value of d, or 0.15 m. Figure 44 shows the Nyquist plot of this system. No limit cycle is predicted for this value of A or any less.

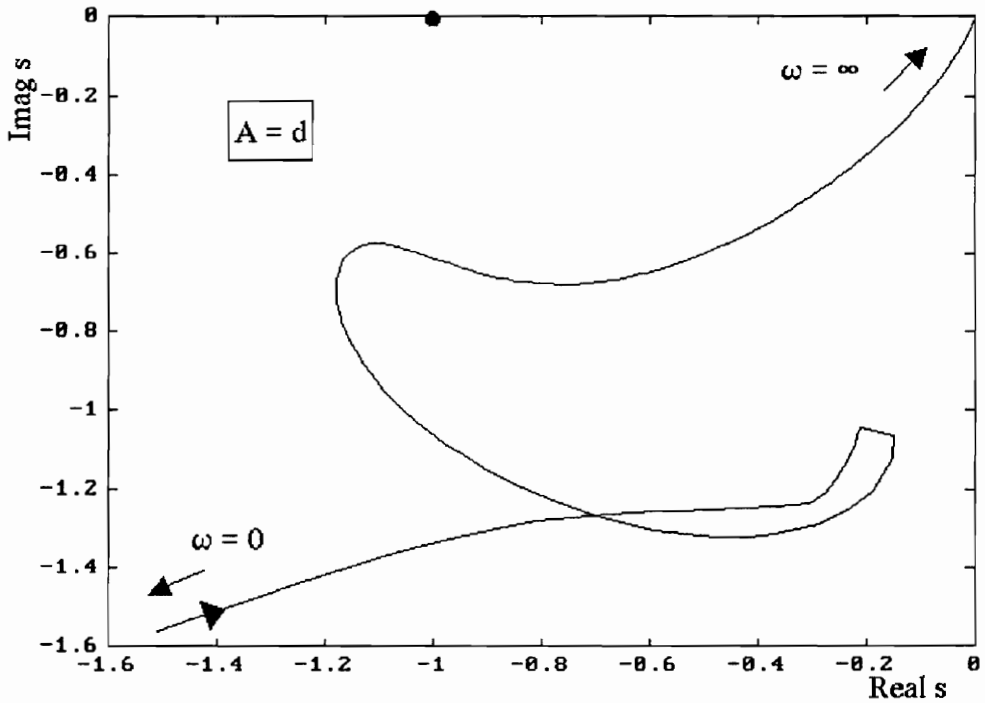

Figure 44 Nyquist plot of System with Stiff Spring Function

Figure 45 shows a comparison of Figure 42 and 44. The stiff spring function has subtracted phase throughout the plot (rotated it clockwise around the origin). This behavior is undesirable since the subtraction of phase moves the Nyquist plot closer to the critical point.

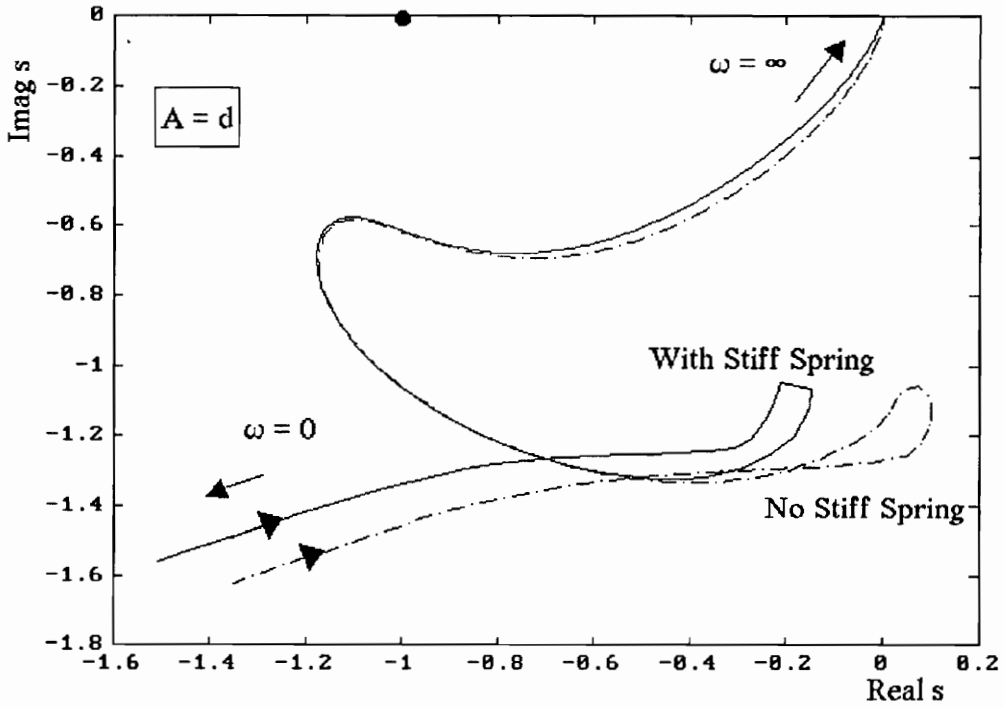

Figure 45 Nyquist Plots Showing Effect of Stiff Spring

Finally consider the system with the position/velocity nonlinearity control loop to manage the proof-mass as shown in Figure 19. The Nyquist plot for this system is shown in Figure 46. By comparing the plots in Figures 42 and 46, it can be seen that the nonlinear feedback has altered the curve in a region away from the critical point. Unlike the stiff spring function, the phase and magnitude of the Nyquist plot remains virtually unchanged throughout the rest of the plot. This analysis suggests that the system with the position/velocity nonlinearity control law will not introduce limit cycles.

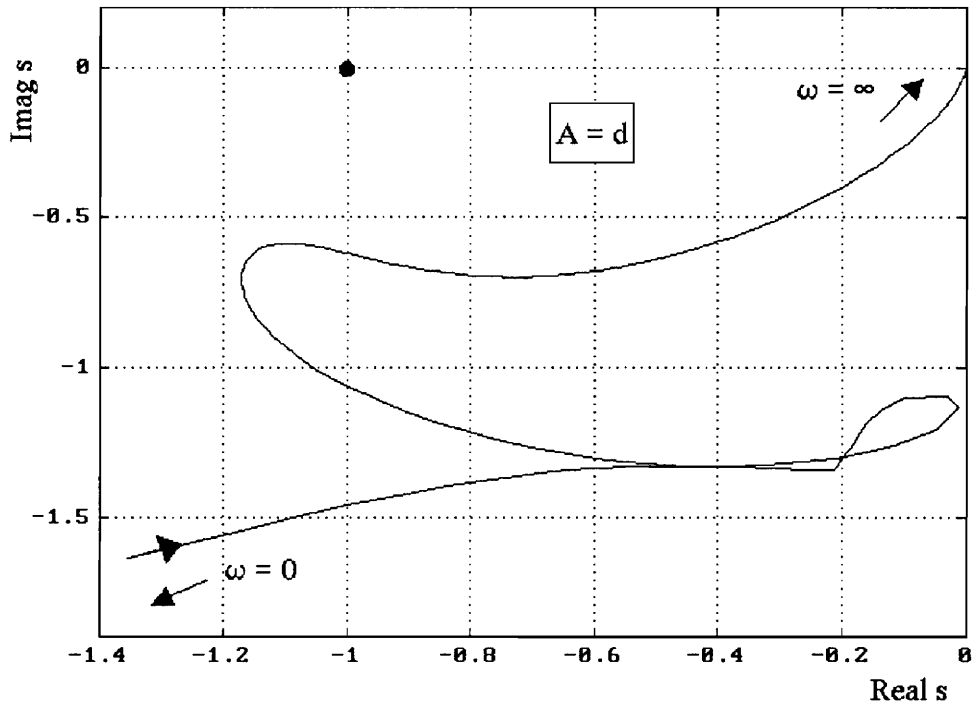

Figure 46 Nyquist Plot for the System with Position/Velocity Nonlinear Feedback

In conclusion, it was found that the presence of the command limiter does not cause the system to experience limit cycles if the system is not conditionally stable on the vibration suppression gains. This is usually the case since the closed loop poles of the structure are close the open loop poles and the root locus would not normally cross the imaginary axis in the loci in between. It was shown the impact on the Nyquist plots due to the nonlinear feedback is minimal and in an area not close to the -1+j0 critical point. Therefore the nonlinear feedback does not tend to induce limit cycles.

CHAPTER 7

CONCLUSIONS

By matching a proof-mass actuator's transfer function to the stroke/force saturation curve, the actuator is designed to produce maximum force at all frequencies as determined by the stroke and force nonlinearities. In this text, the performance of an actuator designed in this manner was assessed. The performance was found to be related to the size of the operating region and the vibration suppression capabilities. Nonlinear control was shown to expand this operating region without sacrificing equivalent damping. The position/velocity nonlinearity was found to perform better than the stiff spring nonlinearity because it predicted stroke saturation more accurately.

It was argued that the performance of the actuator depended on the relation of the lowest modal frequency of the structure and the saturation break frequency. If the frequency of this saturation break frequency is matched to the structural mode, then the performance improves only if nonlinear control is employed. Through the use of this nonlinear control, it was shown that performance of a low mass actuator could out-perform a large mass actuator. Once the relation between the saturation break frequency and the structural mode is established, the designer can choose two of the three basic actuator parameters: F_{Max}, m, and d. It was suggested that F_{Max} and d should be made as large as possible. Interestingly, the

improvements of trading mass for stroke are only seen in a actuator where the nonlinear control employed.

The limit cycle analysis concluded that the force saturation could cause limit cycles if vibration suppression was attempted on a mode whose frequency did not match the saturation break frequency. Instead, by choosing the ratio of K_{ps}/K_{vs} to be much greater than the saturation break frequency, the possibility of limit cycles is avoided. The harmonic balance analysis showed that the nonlinear control did not tend to induce limit cycles.

The results in this text depend of several fundamental assumptions. One type has to do with model approximations such as no friction in the actuator, ideal sensors, and finite modal approximation of the structure. It can be assumed that violations of this type of assumption will only degrade the performance, but the overall results will still apply. Another assumption, is that the structure has very little open loop damping and that the closed loop damping requirements are modest (5%-20%). If this assumption is not applicable, then the phase compensation techniques cannot be applied. Since the design of the vibration suppression loops is crucial to all of the analysis in this text, the results cannot apply in this case. Finally, this analysis is dependent on the structure of the control. If, for example, the vibration suppression gains are replaced with dynamic compensators, this system cannot be guaranteed to perform in the manner described in this text.

Future work could include the development of a performance function that could be used for a multi-modal structure. Also, the simulations in this text were of the initial condition type. The performance of a system could be studied in response to sinusoidal disturbances to the structure. The next logical step for this research is to use the performance function as a cost function to find an optimal control for the

actuator. Finally and above all, there needs to be experimental verification of not only the nonlinear control, but also the limit cycle analysis.

REFERENCES

Anderson, W. W., and Groom, N. J., "The Angular Momentum Control Device (AMCD) and Potential Applications," NASA TW D-7866, March, 1975.

Atherton, D. P., Nonlinear Control Engineering, New York : Van Nostrand Reinhold, 1984.

Celano, T., "The Linear DC Motor as a Proof Mass Actuator for Vibration Suppression in Large Space Structures," Master's Thesis, Virginia Polytechnic Institute and State University, Blacksburg, VA, 1989.

Clark, W. W. and Robertshaw, H. H., "A Planar Comparison of Actuators for Vibration Control of Flexible Structures," *Proceedings of the 30th Structures, Structural Dynamics, and Materials Conference*, Mobile, AL, April 1989.

Ham, F., S. Greeley, and B. Henniges, "Active Vibration Suppression for the Mast Flight System," *IEEE Control Systems Magazine*, Vol. 9, 1989, pp. 85-90.

Ide, E. N., "Evaluation of LDCM Actuators for Control of Large Space Structures," Master's Thesis, Virginia Polytechnic Institute and State University, Blacksburg, VA, 1988.

Lindner, D.K., Celano, T., and Ide, E., "Vibration Suppression Using a Proofmass Actuator Operating in Stroke/Force Saturation," *ASME Journal of Vibration and Acoustics*, 1991.

Nurre, G. S., Ryan, R. S., Scofield, H. N., Sims, J. L., "Dynamics and Control of Large Space Structures," *Journal of Guidance, Control, and Dynamics*, Vol. 7, Sept-Oct 1984, pp. 514-526.

Politansky, H., Pilkey, W. D., "Suboptimal Feedback Vibration Control of a Beam with a Proof-Mass Actuator," *Journal of Guidance, Control, and Dynamics*, Vol. 12, Sept-Oct 1989, pp. 691-697.

Haviland, J. K., Lim, T. M., Pilkey, W. D., Politansky, H., "Control of Linear Dampers for Large Space Structures," *Journal of Guidance, Control, and Dynamics*, Vol. 13, Mar-Apr 1990, pp. 234-240.

Sulla, J., Juang, J., and Horta, L., "Analysis and Application of a Velocity Command Motor as a Reactor Mass Actuator," *Proceedings of the AIAA Dynamics Specialist Conference*, Long Beach, CA, 1990, pp. 360-370

Özgüner, Ü., Yurkovich S., Martin J., and Kotnik P., "A Laboratory Facility for Flexible Structures Control Experiments," *Proceedings of the Sixth VPI&SU Symposium on Dynamics and Control of Large Space Structures*, Blacksburg, VA, June 1987.

APPENDIX

PROGRAM FLOWCHARTS

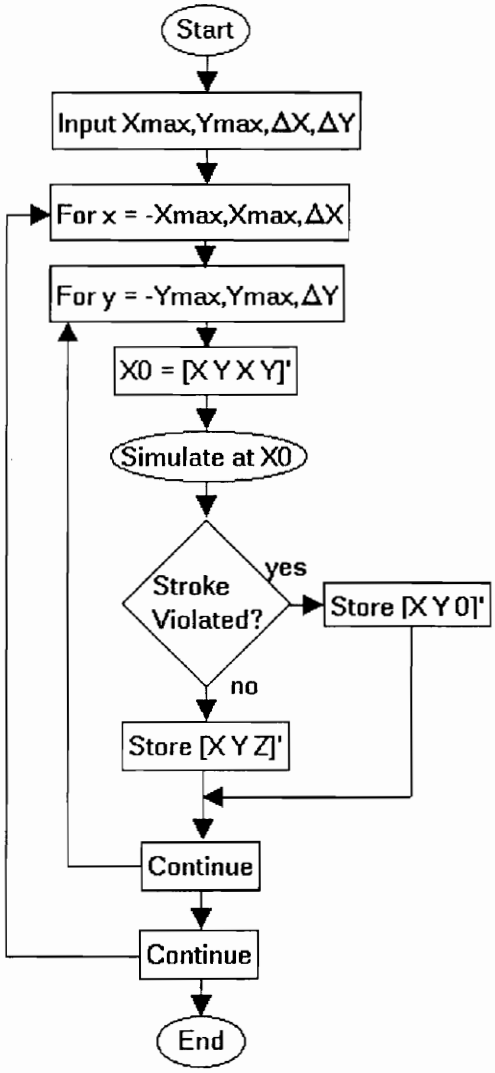

Flowchart of Main Calling Routine for Performance Function Evaluator

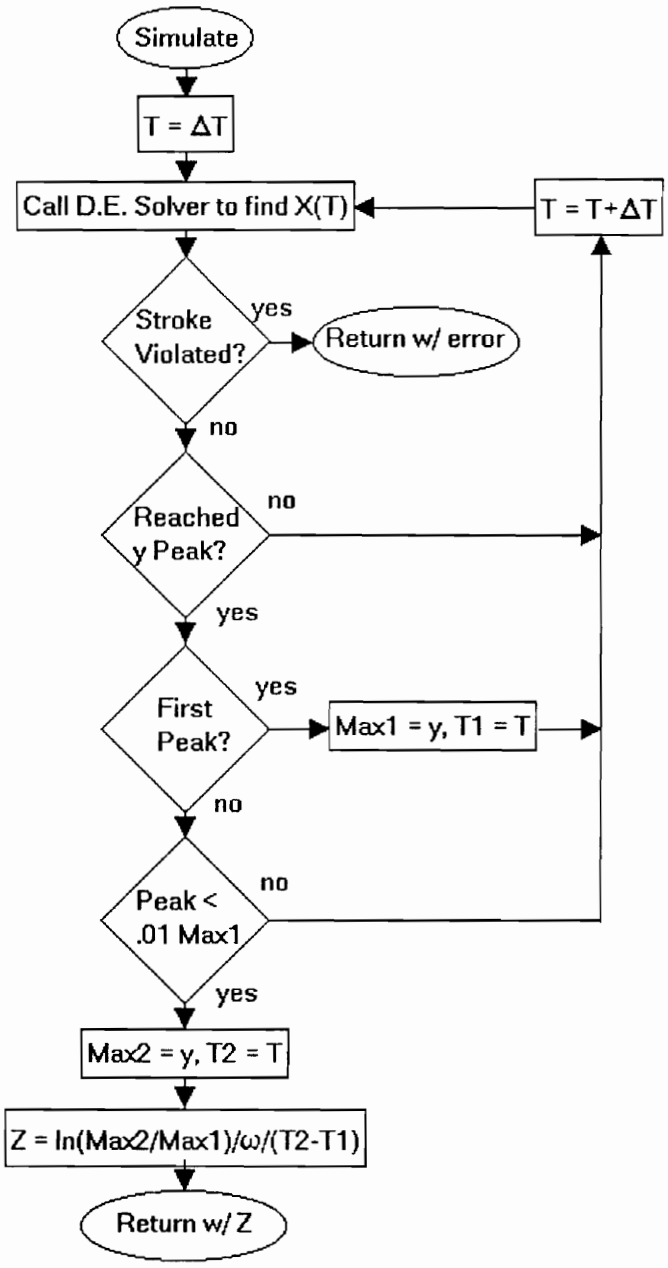

Subroutine to Calculate Equivalent Damping

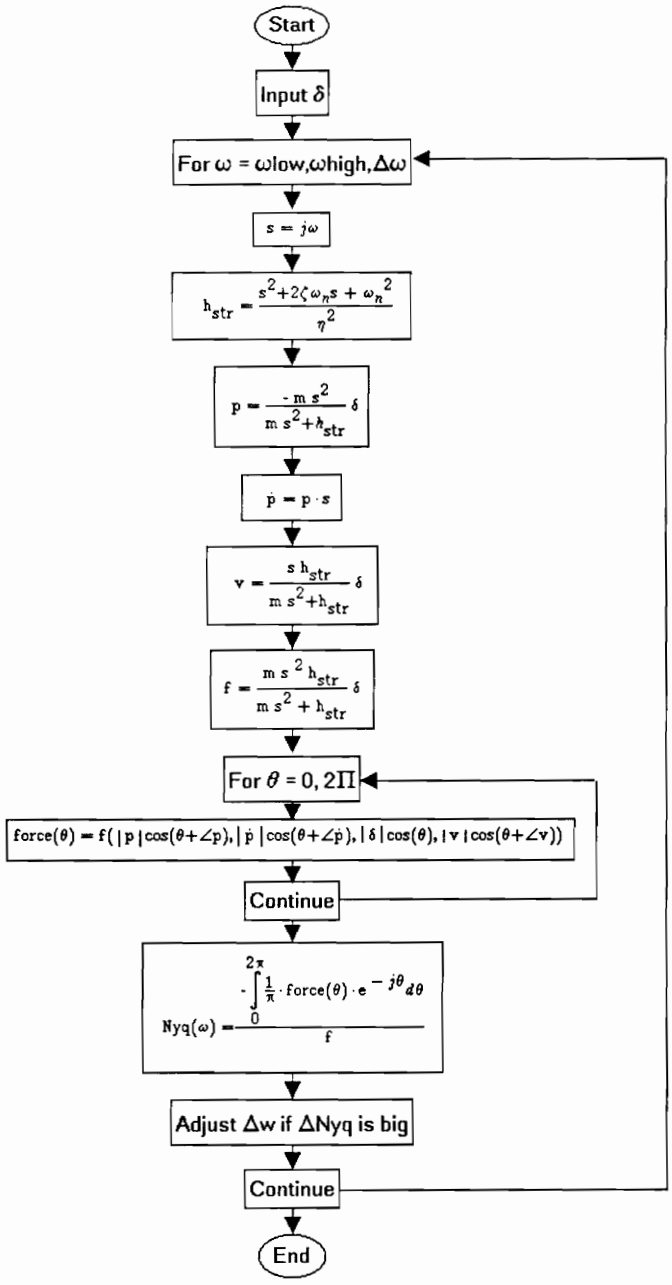

Flowchart of Nyquist Plot Algorithm

VITA

Mr. Zvonar was born on March 1, 1968 and grew up in Mt. Lebanon, Pennsylvania a suburb of Pittsburgh. In 1986, he entered Vi rginia Polytechnic Institute and State University as a Bachelor of Science candidate in the College of Engineering. After beginning his studies in the Bradley Department of Electrical Engineering, he was awarded a Bradley Scholarship. While an undergraduate, Greg was a member of Pi Lambda Phi fraternity and was invited into Tau Beta Pi and Eta Kappa Nu.

After graduating Magna Cum Laude in June of 1990, Greg enrolled into the graduate program at Virginia Tech. Upon his entry into the Electrical Engineering program he was awarded a prestigious Bradley Fellowship. After completing his studies in December of 1991, he began working for International Business Machines in Charlotte, North Carolina.

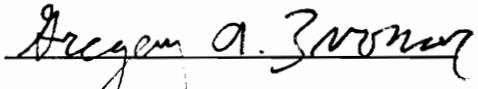

Gregory A. Zvonar